A Novel Integral Interconnection Damping Assignment Passivity-Based Control Approach for Underactuated Inverted Pendulum System

Minh-Duc Tran [1], Vinh-Hao Nguyen [2*]
[1, 2] Department of Control Engineering and Automation, Ho Chi Minh City University of Technology (HCMUT), Viet Nam
National University Ho Chi Minh City, Ho Chi Minh City, 700000, Vietnam
Email: [1] tmduc.sdh222@hcmut.edu.vn, [2] vinhhao@hcmut.edu.vn
*Corresponding Author

***Abstract*—This study explores an application of robust nonlinear control to an underactuated inverted pendulum system (UIPS), a type of underactuated mechanical system, by first transforming the perturbed system into a form of a port-controlled Hamiltonian system (PCH), then utilizing the Interconnection and Damping Assignment Passivity-Based Control (IDA-PBC) methodology to achieve the stabilization of an unperturbed closed-loop PCH system with an assigned energy function that qualifies as a Lyapunov candidate at the unstable equilibrium point. From there, the problem of robustification of IDA-PBC for a perturbed closed-loop PCH system with the state-dependent input matrix of the UIPS, subject to constant matched disturbances, is addressed by adding an outer-loop controller with an additional state. This results in a new system that preserves the framework of a PCH system, rejects the disturbance, and has a new energy function that again serves as a Lyapunov function at the desired equilibrium point. This proposed methodology is called integral IDA-PBC (iIDA-PBC). The effectiveness and applicability of the proposed method are thoroughly assessed through numerical simulations and experimental validation on the UIPS. The results demonstrate the method's proficiency in handling the system's constant matched disturbances and model inaccuracies, underscoring the potential of iIDA-PBC for broader applications in systems facing similar control challenges.**

Keywords*—*Underactuated Inverted Pendulum System; IDA-PBC; Robust Nonlinear Control; Hamiltonian Systems; Disturbance Rejection.

I. INTRODUCTION

Using a well-known underactuated system like the underactuated inverted pendulum system (UIPS) is often the preferred choice for researchers to explore and validate new control strategies, study chaos theory, and more. This is due to its highly nonlinear nature and underactuation, where the number of inputs is fewer than the degrees of freedom, making control strategies particularly challenging for the underactuated components. Recent studies demonstrate that UIPS is in fact able to work in the mentioned fields, and is used as a practical system to verify the research methodology. For few examples, O. Saleem and colleagues developed an adaptive fractional-order linear quadratic regulator for the UIPS and demonstrated its effectiveness through experiments [1]. Similarly, T. Li et al. (2024) investigate the effects of the fractional Gaussian noise excitation for the UIPS [2]. New intelligent methods have also been researched and applied, such as the RBF-ARX model-based predictive controller [3], while optimal robust adaptive fuzzy techniques were employed to enhance control performance [4]. Additionally, the Takagi-Sugeno fuzzy methodology has been extensively studied and implemented in multiple works [5]-[10]. Furthermore, chaotic behavior analyses have been conducted in several studies to explore complex system dynamics [11]-[15]. Besides, it also serves as a valuable model for developing new mechanical systems, such as Segways [16], [17], human posture control systems [18], [19]-[22], self-balancing robots [23]-[25]. Based on this analysis, we target to utilize the UIPS to qualify our controller proposal, namely Integral Interconnection and Damping Assignment Passivity-Based Control (iIDA-PBC) technique.

Regarding IDA-PBC, it is a control method for nonlinear systems that stabilize dynamic systems by designing them to achieve the desired energy structure. The technique modifies the system's dynamics to embed a target closed-loop behavior, typically by assigning a Hamiltonian structure (e.g. PCH) to the system, allowing the energy function to act as a Lyapunov function for stability. For PCH, it is a specific type of physical system used in control theory and system dynamics that incorporates both energy exchange and Hamiltonian mechanics. This framework models systems that can exchange energy with their environment through "ports," which are interfaces for input and output.

Several studies on the mentioned approach, devoted to the class of underactuated systems have appeared in literature and industry. For instance, P. Borja (2024) [26] studies about how to remove the PDEs from his control design for IDA-PBC, or Mattioni studies the controller in discrete models and with time delays [27][28]. Moreover, in [77][78], a new approach called cbI-PBC is introduced as a variation of passivity-based control, involving deeper analysis within the internal system.

On top of that, IDA-PBC has been studied for many advanced models such as autonomous underwater vehicles [29]-[31], unmanned aerial vehicles [32]-[36],induction motors [37]-[39], permanent magnet synchronous motor [40]-[43], underactuated systems [44]-[49], robot [50]- [53], hybrid electric vehicles [54][55], power systems [56]-[63], and so on. In numerous practical scenarios, the system's state may not be directly measurable. To address this challenge, studies in [79] and [82] propose an approach for designing an observer to estimate the system's state effectively.

The IDA-PBC is effective in controlling unperturbed nonlinear systems; however, it does not maintain the desired equilibrium point when disturbances occur. These disturbances can be categorized into two types: matched and unmatched. Matched disturbances are related to modeling errors or any disturbance that can be mapped through the input matrix, whereas unmatched disturbances cannot be mapped through the input matrix and act independently of the control input.

Researchers have started addressing the problem of rejecting such disturbances after achieving a stable closed-loop system at the equilibrium point using IDA-PBC. Some approaches involve adaptive control [36] or the integration of an integral action, known as Integral Interconnection and Damping Assignment Passivity-Based Control (iIDA-PBC) [64][65]. Significant efforts have been made in this area. For instance, E. Franco and colleagues in [66] explored the implementation of iIDA-PBC for underactuated systems with actuator dynamics and uncertain coupling. In 2015, M. Ryalat et al. proposed an iIDA-PBC PID-like control approach [67]. However, these techniques introduce additional partial differential equations (PDEs), which can be challenging to solve. To address this issue, researchers [68]-[71] proposed integrating an integral action into the IDA-PBC framework to counteract disturbances without requiring additional PDEs. However, this method only addresses matched disturbances under the condition that the input matrix is constant. Furthermore, it requires a new coordinate transformation for underactuated systems to apply their proposed method.

In this paper, we present a step-by-step procedure for designing an IDA-PBC on an UIPS, omitting the solving PDEs proof but providing remarks for those who wish to apply it to other systems. Next, we propose a different formulation of the iIDA-PBC methodology for handling constant matched disturbances. This approach does not introduce any additional PDEs, relaxes the requirement for a constant input matrix, and avoids the necessity of transforming to a new coordinate system. Finally, we demonstrate the effectiveness of the proposed method through both simulation and experimental results. The results show that constant matched disturbances are rejected. Additionally, some limitations are discussed, highlighting areas for future development.

The organization of this paper is structured into five parts: First, a brief introduction to the IDA-PBC methodology for the PCH system is provided. Second, the dynamics of the UIPS with constant matched disturbances are presented, including the step-by-step design of the IDA-PBC on the UIPS, the effects of the mentioned disturbances on the closed-loop system, and the problem statement along with the proposed solution. Third, the methodology is introduced, including the stability proof and a visualized tuning procedure. Fourth, the results from both simulations and experiments are presented. Finally, the paper concludes with final remarks, a discussion of ongoing work related to the system, and suggestions for future research.

Notation 1. In this manuscript, we use the notation as follows: $I_n$is a $n \times n$identity matrix, $0_{n\times m}$ denotes a $n \times m$that contains only zero in each of its entry. For $q \in \mathbb{R}^n$, we define $\|q\|_K^2 = q^T K q$ for $K \in \mathbb{R}^{n\times n}$ and $K = K^T > 0$. For $p \in \mathbb{R}^{n\times m}$, the symbol $\|p\|$ is its induced norm. The gradient of a mapping $T(q): \mathbb{R}^n \to \mathbb{R}$ is denoted as $\nabla T(q) \triangleq (\partial T/\partial q)^T$.

Notation 2. The arguments of the functions are sometimes omitted for the availability of spaces and simplification.

TABLE I. LIST OF ABBREVIATIONS

Abbreviation	Full Description
UIPS	Underactuated inverted pendulum system
PDEs	Partial differential equations
PCH	Port-controlled Hamiltonian
IDA-PBC	Interconnection and damping assignment - Passivity based control
iIDA-PBC	Integral interconnection and damping assignment - Passivity based control
NMAE	Normalized Mean Absolute Error
NRMSE	Normalized Root Mean Squared Error

II. MATHEMATICAL MODELING

A. Overview of The Port-Controlled Hamiltonian System and the Design of the IDA-PBC

An underactuated system with n-DOFs, is described in the form of the port-controlled Hamiltonian as follows:

$$\begin{bmatrix} \dot{q} \\ \dot{p} \end{bmatrix} = \begin{bmatrix} 0 & I \\ -I & -D \end{bmatrix} \begin{bmatrix} \nabla_q H(q,p) \\ \nabla_p H(q,p) \end{bmatrix} + \begin{bmatrix} 0 \\ G(q) \end{bmatrix} u \tag{1}$$

Where the control input $u \in \mathbb{R}^m$, which applies to the input matrix $G(q) \in \mathbb{R}^{n\times m}$ with $rank(G) = m(m < n)$. The system states $q \in \mathbb{R}^n$ and the momenta $p = M_t(q)\dot{q} \in \mathbb{R}^n$, the physical damping $D = D^T \geq 0$.

The mechanical energy function of the system,

$$H(q,p) = \frac{1}{2} p^T M_t^{-1}(q) p + \Omega(q) \tag{2}$$

is characterized by the kinetic term, associated with the positive definite inertia matrix $M_t = M_t^T \succ 0$, and the potential energy $\Omega(q)$. The partial derivative of $H(q,p)$ with respect to q is $\nabla_q H(q,p)$, and the partial derivative of $H(q,p)$ with respect to p is $\nabla_p H(q,p)$.

As in [72], to achieve the goal of stabilizing the system at the desired equilibrium $(q,p) = (q^*, 0)$, the energy function (3) should be shaped in the new form:

$$H_d(q,p) = \frac{1}{2} p^T M_d^{-1} p + \Omega_d(q) \tag{3}$$

For which, the new potential energy $\Omega_d(q)$should admit a strict minimizer in $q^*$and verify the conditions $\nabla_p \Omega_d(q^*) = 0$ and $\nabla_p^2 \Omega_d(q^*) > 0$, and the inertial matrix $M_d(q) = M_d^T(q) \succ 0$.

The target closed-loop system has the form:

$$\begin{bmatrix} \dot{q} \\ \dot{p} \end{bmatrix} = \begin{bmatrix} 0 & M_t^{-1} M_d \\ -M_d M_t^{-1} & J_2 - G K_V G^T - D M_t^{-1} M_d \end{bmatrix} \begin{bmatrix} \nabla_q H_d \\ \nabla_p H_d \end{bmatrix} \tag{4}$$

This is achieved by using the IDA-PBC control law [72] as follows:

$$\begin{cases} u = u_{es} + u_{di} \\ u_{es} = G^{+}\left[\nabla_q H - M_d M_t^{-1} \nabla_q H_d + J_2 \nabla_p H_d\right] \\ u_{di} = -K_V G^T \nabla_p H_d \end{cases} \tag{5}$$

The suitable inertia matrix $M_d(q)$ and $\Omega_d(q)$ are verified for the partial differential equations by matching (4) and (1), the result is as follows:

$$\begin{cases} G^{\perp}\left(\nabla_q \Omega - M_d M_t^{-1} \nabla_q \Omega_d\right) = 0 \\ G^{\perp}\left(\nabla_q H - M_d M_t^{-1} \nabla_q (p^T M_d^{-1} p) + 2 J_2 \nabla_p H_d\right) = 0 \end{cases} \tag{6}$$

Where $G^{+}(q) = (G^T G)^{-1} G^T(q)$ is the left pseudo-inverse matrix, the damping gain $K_V = K_V^T \succ 0$, the free matrix $J_2(q,p) = -J_2^T(q,p)$, $G^{\perp}(q)$ is the full rank left annihilator of $G(q)$. The input $u_{es}$is called the energy shaping control law, which first shape the in to the form (4) without the term $G K_V G^T(q)$, then the input u_{di}, called damping injection law, adds the remaining term.

Taking the time-derivative of $H_d(q,p)$ yields:

$$\dot{H}_d = -\nabla_p H_d^T \left(G K_V G^T + D M_t^{-1} M_d\right) \nabla_p H_d \le 0 \tag{7}$$

From (7), $(q,p) = (q^*, 0)$ is the stable equilibrium of the closed-loop system (4) [72]. Furthermore, it is asymptotically stable if, according to Lasalle's theorem, the largest invariant set under the system (4) satisfies the following:

$$\left\{(q,p) \in \mathbb{R}^{2n} \middle| \dot{H}_d(q,p) = 0\right\} = \{(q^*, 0)\} \tag{8}$$

If $y_d \triangleq G^T \nabla_p H_d$ is detectable, for the case $D = 0$ in (7), as $y_d = 0 \Rightarrow (q,p) = (q^*, 0)$. For clearance, we have $\dot{H}_d(q,p) \le y_d^T u_{di}$, in which y_d is the passive output of (4) and the control u_{di} defined as in (5) preserves passivity.

Remark 1. The current form of (6) includes terms such as the system's inertia matrix, kinetic energy, and the skew-symmetric matrix, all of which are functions of q and p, making the equation nonlinear and coupled. Solving this type of partial differential equation requires a specific structure to derive a solution. In this paper, the detailed proof of the steps for solving (6) is omitted due to its length and because it primarily follows well-established methods, as our focus is on addressing the rejection of the additive matched disturbance in the perturbed system, which will be mentioned in sequel. Readers seeking a deeper understanding of the proof are encouraged to refer to [72] and [73] for comprehensive insights.

B. *The System Dynamic of the UIPS*

The schematic of the UIPS is captured in Fig. 1. The dynamic of the UIPS is of the form [74], [69].

$$\begin{bmatrix} \ddot{x} \\ \ddot{\theta} \end{bmatrix} = \begin{bmatrix} f_1(x, \dot{x}, \theta, \dot{\theta}) \\ f_2(x, \dot{x}, \theta, \dot{\theta}) \end{bmatrix} + \begin{bmatrix} g_1(\theta) \\ g_2(\theta) \end{bmatrix} (v - d) \tag{9}$$

Where $x, \dot{x}, \theta, \dot{\theta} \in \mathbb{R}$ are the system's states $f_1, f_2 \in \mathbb{R}$ and $g_1, g_2 \in \mathbb{R}$ are differentiable, $v \in \mathbb{R}$ is the control input, and $d \in \mathbb{R}$ is the disturbance to be rejected, which is not known.

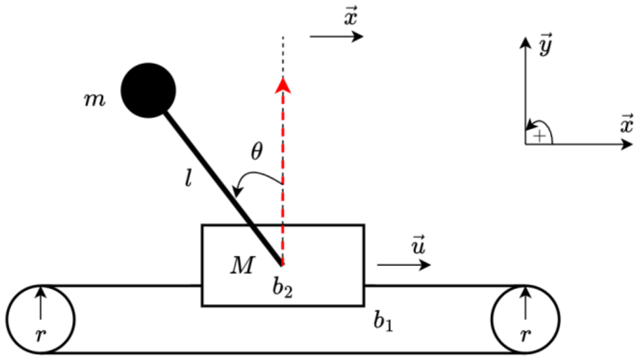

Fig. 1. Schematic of the UIPS

$$f_1 = \frac{ml\dot{\theta}^2 \sin\theta - \left(b_1 + \frac{B}{r} + \frac{k_t^2}{Rr}\right)\dot{x} + \frac{1}{l}\cos\theta\left(mgl\sin\theta - b_2\dot{\theta}\right)}{M + J/r + m\sin^2\theta}$$

$$g_1 = \frac{k_t/R}{M + J/r + m\sin^2\theta}$$

$$f_2 = \frac{\frac{1}{ml^2}\left(M + m + \frac{J}{r}\right)\left(mgl\sin\theta - b_2\dot{\theta}\right) - m\dot{\theta}^2\sin\theta\cos\theta - \frac{1}{l}\left(b_1 + \frac{B}{r} + \frac{k_t^2}{Rr}\right)\dot{x}\cos\theta}{M + J/r + m\sin^2\theta}$$

$$g_2 = \frac{\frac{1}{l}\cos\theta\frac{k_t}{R}}{M + J/r + m\sin^2\theta}$$

$$g_d(q) = \frac{k_t/R}{M + J/r + m\sin^2\theta} > 0$$

Where M and m are, respectively, the mass of the cart and the pendulum's mass, l is the length of the pendulum. J, R, k_t, B are the inertia, resistance of the coil, torque constant and friction of the DC motor, respectively. r is the radial of the pulley for the force transition from the rotation of the motor shaft to the cart. b_1 and b_2 are the torque friction of the cart and the pendulum of the system.

C. *The Port Controlled Hamiltonian System of the UIPS*

Applying the feedback equivalence to (9) as follows [75].

$$v = \frac{-f_1 + u_1}{g_1} \tag{10}$$

The system (9) is of the form

$$\begin{cases} \ddot{x} = u_1 - g_d d \\ \ddot{\theta} = \frac{g}{l}\sin\theta - \frac{b_2}{ml^2}\dot{\theta} + \frac{1}{l}\cos\theta\, u_1 - \frac{g_d d}{l}\cos\theta \end{cases} \tag{11}$$

The system (11) can be inferred as the port-controlled Hamiltonian system

$$\begin{bmatrix} \dot{q} \\ \dot{p} \end{bmatrix} = \left(\begin{bmatrix} 0 & I \\ -I & 0 \end{bmatrix} - \begin{bmatrix} 0 & 0 \\ 0 & D \end{bmatrix}\right)\begin{bmatrix} \nabla_q H \\ \nabla_p H \end{bmatrix} + \begin{bmatrix} 0 \\ G(q) \end{bmatrix} u_1 - \begin{bmatrix} 0 \\ G(q) \end{bmatrix} g_d d \tag{12}$$

Where $q = [x \quad \theta]^T$, $p = [\dot{x} \quad \dot{\theta}]^T$are the states of the port-controlled Hamiltonian system. The system energy is of the form $H(q,p)=\frac{1}{2}p^T M_t^{-1} p+\Omega(q)$, the potential energy $\Omega(q)=\frac{g}{l}\cos\theta$, $D=\begin{bmatrix}0 & 0\\ 0 & \frac{b_2}{ml^2}\end{bmatrix}$, and $G(\theta)=\begin{bmatrix}1\\ (1/l)\cos\theta\end{bmatrix}$.

Remark 2. In (11), the underactuation term $\ddot{\theta}$ contains the friction part $-\frac{b_2}{ml^2}\dot{\theta}$, which cannot be directly removed by the input $\frac{1}{l}\cos\theta\, u_1$ in all the operation range of the pendulum. As can be seen in (7), the dissipation matrix D, contains all the friction type, contributes to the stability of the system. This is the feature that makes this approach different than other nonlinear controllers.

D. Formulation of IDA-PBC for the UIPS

The IDA-PBC control law [72] with $d=0$ of the system (12) is given as follows

$$u_1 = u_{es}+u_{di}+u \tag{13}$$

Such that

- The control input u is arbitrary. For IDA-PBC, this equals to zero.
- $K_V=K_V^T>0$ and $M_t=\begin{bmatrix}1 & 0\\ 0 & 1\end{bmatrix}$
- $M_d(\theta)=M_d^T(\theta)=\begin{bmatrix}k\cos\theta & \frac{kb}{2}\cos^2\theta\\ \frac{kb}{2}\cos^2\theta & \frac{kb^2}{3}\cos^3\theta\end{bmatrix}$
- $\Omega_d(q)=\frac{3a}{kb}(\sec^2\theta-1)+\frac{P}{2}\left[x-\frac{3}{b}\ln(\sec\theta+\tan\theta)\right]^2$ satisfies $q^*=\operatorname{argmin}\Omega_d(q)$
- u_{es} and u_{di} is defined in (4).
- $J_2(q,p)=-J_2^T(q,p)=p^T M_d^{-1} G\phi W_1$

Where $\phi(\theta)=k\sin\theta$ with $k>0$

$$W_1=\begin{bmatrix}0 & 1\\ -1 & 0\end{bmatrix}$$

These functions and parameters are verified for all $(q,p)\in\mathbb{R}^4$ the partial differential equations (PDEs).

$$G^{\perp}\left(\frac{1}{2}M_d M_t^{-1} e_1 \nabla_q H_d + J_2(q,p)\right)M_d^{-1}p=0 \tag{14}$$

$$G^{\perp}\left(\nabla_q\Omega - M_d M_t^{-1}\nabla_q\Omega_d\right)=0 \tag{15}$$

Where $e_r\in\mathbb{R}^2$ is the r-th vector of the standard Euclidian basis and $G^{\perp}(\theta)$ is the full rank left annihilator of $G(\theta)$, which means that $G^{\perp}G(\theta)=0$.

The desired closed-loop dynamic ($u=0$) is thus of the form as in (4). We recall the format of the closed-loop system:

$$\underbrace{\begin{bmatrix}\dot{q}\\ \dot{p}\end{bmatrix}}_{\triangleq\dot{x}_p}=\underbrace{\begin{bmatrix}0 & M_t^{-1}M_d\\ -M_d M_t^{-1} & J_2-GK_VG^T-DM_t^{-1}M_d\end{bmatrix}}_{\triangleq\xi(q,p)}\underbrace{\begin{bmatrix}\nabla_q H_d\\ \nabla_p H_d\end{bmatrix}}_{=\nabla H_d} \tag{16}$$

We define new term, that is used for the stability proof in the latter section as follows: $R_d\triangleq\begin{bmatrix}0 & 0\\ 0 & GK_VG^T\end{bmatrix}$ $x_p\triangleq\begin{bmatrix}\dot{q}\\ \dot{p}\end{bmatrix}$ $\nabla H_d\triangleq\begin{bmatrix}\nabla_q H_d\\ \nabla_p H_d\end{bmatrix}$, $G_c(q)\triangleq\begin{bmatrix}0\\ G(q)\end{bmatrix}$, $J_d\triangleq\begin{bmatrix}0 & M_t^{-1}M_d\\ -M_dM_t^{-1} & J_2-DM_t^{-1}M_d\end{bmatrix}$, and $\xi(q,p)\triangleq J_d(q,p)-R_d(q)$.

The new system's energy of the UIPS is of the form:

$$\begin{aligned}H_d(q,p)=\frac{1}{2}p^T&\begin{bmatrix}k\cos\theta & \frac{kb}{2}\cos^2\theta\\ \frac{kb}{2}\cos^2\theta & \frac{kb^2}{3}\cos^3\theta\end{bmatrix}^{-1}p\\ &+\frac{3a}{kb}(\sec^2\theta-1)\\ &+\frac{P}{2}\left[x-\frac{3}{b}\ln(\sec\theta+\tan\theta)\right]^2\end{aligned} \tag{17}$$

The briefly procedure to derive the parameters for the control law (13) after for solving (14) and (15) in [73] is summarized as follows:

TABLE II. PARAMETER DERIVATION FOR IDA-PBC

Calculation Steps for IDA-PBC Parameters
Step 1. Start at system (11) where $d=0$. Calculate the gradient of $\nabla\Omega(q)$, and find the full-rank left annihilator $G^{\perp}(\theta)$ of $G(\theta)$. Note that $M_t=I$.
Step 2. Choose $\phi(\theta)=k\sin\theta$ with $k>0$ and determine the inertia matrix $M_d(\theta)$ in the following form $M_d(\theta)=\int_0^{\theta}G(s)\,\phi(s)G^T(s)ds+M_d^0$ Where M_d^0 is the constant matrix that eliminates all the constants in the matrix derived from the integral term.
Step 3. Define new input matrix $\tilde{G}^{\perp}(\theta)=\eta(\theta)G^{\perp}(\theta)$, and calculate $\eta(\theta)=\frac{\rho}{G^{\perp}(\theta)M_d(\theta)e_2}$, ρ is a constant.
Step 4. Find the potential energy $\Omega_d(q)$ as follows: $\Omega_d(q)=\frac{1}{\rho}\int_0^{\theta}\tilde{G}^{\perp}(s)\,\nabla\Omega(s)ds+\Theta(z(q))$ Where $\Theta(z(q))=\frac{1}{2}\left(z(q)-z(q^*)\right)^T P\left(z(q)-z(q^*)\right)$ and $z(q)=x-\frac{1}{\rho}\int_0^{\theta}\tilde{G}^{\perp}(s)\,M_d(s)e_2ds$.
Step 5. Compute the skew-symmetric matrix $J_2(q,p)=-J_2^T(q,p)=p^TM_d^{-1}G\phi W_1$ with $W_1=\begin{bmatrix}0 & 1\\ -1 & 0\end{bmatrix}$

Remark 3. In order to follows the procedure, some conditions must satisfy. First, the system must have an underactuation degree of one. For instance, our UIPS has 2 DOF with 1 input, satisfying this condition. However, if the UIPS has 2 pendulums, it becomes a 3 DOF system with 1 input, resulting in an underactuation degree of two, which makes the mentioned method in [73] inapplicable. Second, the system in the form of (10) must have an inertia matrix M_t equals to an identity matrix of the same size. This condition is crucial for (14) to be parameterized in order to find $M_d(q)$. Moreover, for practical applications, having an arbitrary constant matrix M_t is insufficient because in the PCH system, the states are defined as $q=M_t[x\quad\theta]^T$ and $p=M_t[\dot{x}\quad\dot{\theta}]^T$, meaning the states cannot be directly measured unless it's an identity matrix. However, this is not the serious case when the feedback equivalent (10) helps to solve this problem.

Third, the choice of $\phi(\theta)$ in step 3 to achieve a suitable desired inertia matrix $M_d(q)$ may restrict its domain. For example, our choice of $M_d(\theta) = M_d^T(\theta) \succ 0$ is limited to being a positive definite matrix in $\left(-\frac{\pi}{2}, \frac{\pi}{2}\right)$, meaning the controller in (13) cannot swing up the system from the downward position. However, for some systems, such as a wheeled inverted pendulum, one can choose ϕ to be a constant and follow the remaining steps of the procedure to determine all the parameters for the control law (13), which is capable of performing both swing-up and balancing at its unstable equilibrium point, [76] in section 3.4.1.

E. The Effect of the Matched Disturbance to the UIPS

Recall that after matching equations of system (12) and (16), we obtain (15). Additionally, we have $G^{\perp}G = 0$, so that the matched disturbance does not affect in the solution of the PDEs (14) and (15). In this section, we analyze its effect by recovering the matched disturbance when the system is stable at the equilibrium point $(q^*, 0)$, as follows:

$$G^{\perp}\left(\nabla_q \Omega - G g_d d - M_d M^{-1} \nabla_q \Omega_d\right)(q^*) = 0 \tag{18}$$

From (18), we have:

$$G^{\perp}\left(G g_d d + M_d M^{-1} \nabla_q \Omega_d\right)(q^*) = G^{\perp} \nabla_q \Omega(q^*) \tag{19}$$

Since $\nabla_q \Omega(q^*) = 0$ only if $\theta = k\pi$ with $k \in \mathbb{Z}$, we have the following:

$$G(q^*) g_d(q^*) d + M_d(q^*) M^{-1}(q^*) \nabla_q \Omega_d(q^*) = 0 \tag{20}$$

Calculate (20), we obtain the shifting position:

$$x^* = \frac{2 g_d(\theta^*) d}{Pk} \tag{21}$$

In (21), if the system (16) is affected by a matched disturbance d , the system will stabilize at a new equilibrium position $q^* = (x^*, \theta^*) = (x^*, 0)$.

F. Problem Statement

Consider the perturbed system of the form (16) with the new definition term and $d \neq 0$.

$$\dot{x}_p = \xi(x_p) \nabla H_d(x_p) + G_c(x_p) u - G_c(x_p) g_d(x_p) d \tag{22}$$

The constant disturbance d can be interpreted as the system modeling error, the input losses of power circuits, and frictions. This type of disturbance is referred to as a "matched disturbance," and it causes the desired equilibrium point $(q, p)$of the stable system (16) to shift to a different position. We will demonstrate this shifting phenomenon in the simulation results, where $d \neq 0$ at a specific time after the system has stabilized at the desired equilibrium.

To overcome the problem, many methods have been proposed that introduce an additional state to merge the matched disturbance into the system and still preserve the structure of a PCH system, as in [68]-[71]. Following this approach, in this manuscript, the authors enhance the method that has been introduced in those, as it is only applicable to the systems where $G \in \mathbb{R}^m$ is a constant matrix and requires a coordinate transformation when applied to the underactuated systems.

The dynamic state feedback controller and an additional state for our proposed method is as (23).

$$\begin{cases} u = \hat{u}(x_p, \zeta) \\ \dot{\zeta} = f(x_p, \zeta) \end{cases} \tag{23}$$

Where $\zeta \in \mathbb{R}$, which is part of the new dynamic state feedback, which ensures that the system (10) becomes an unperturbed port-controlled Hamiltonian system with an stable equilibrium point at $(x_p^*, \zeta^*) = (x_p^*, c_2 G_c^T x_p^* - c_1^{-1} c_3^{-1} d)$. This conclusion is clearly presented in Remark 5, following the proof of Proposition 2.

III. METHODOLOGY

In this section, we first present our proposed method for rejecting the matched disturbance of the system, including a step-by-step proof. Next, we present our assumption and lemma, to support stability analysis with an explanation and proof, respectively. Finally, we provide a step-by-step design procedure and a visualized structure for applying the proposed method to the perturbed system (22), followed by comments.

A. Proposition of the iIDA-PBC

Proposition 1: The disturbance rejection input u in (13) for the system (22) of the form (23) is introduced the following.

$$u = -c_1 c_3 g_d \left(c_2 G_c^T x_p - \zeta\right) \tag{24}$$

And the new system state is proposed as follows

$$\dot{\zeta} = G_c^T\left(c_2 \hat{\xi} - c_1 g_d I_n\right) \nabla H_d + c_2 \dot{G}_c^T x_p \tag{25}$$

Where $x_p = [q \quad p]^T \in \mathbb{R}^4$, and tuning parameters $c_1, c_2 \in \mathbb{R}^+$, $c_3 > 0$, and $G_c(q) = [0 \quad G(q)]^T$.

The estimation error is defined as follows

$$\varepsilon \triangleq c_2 G_c^T x_p - \zeta \tag{26}$$

The new closed-loop system is introduced as follows

$$\begin{bmatrix} \dot{x}_p \\ \dot{\varepsilon} \end{bmatrix} = \begin{bmatrix} \xi & -c_1 g_d G_c \\ c_2 G_c^T \tilde{\xi} + c_1 g_d G_c^T I_n & -c_1 c_2 g_d G_c^T G_c \end{bmatrix} \begin{bmatrix} \nabla H_d \\ \nabla L_c \end{bmatrix} \tag{27}$$

With $\tilde{\xi}(q, p) = \xi(q, p) - \hat{\xi}(q, p)$ is the modelling error.

The energy function of $L_c(\varepsilon)$is constructed as follows

$$L_c(\varepsilon) = \frac{1}{2}\left(\varepsilon + \frac{1}{c_1} c_3^{-1} d\right)^T c_3 \left(\varepsilon + \frac{1}{c_1} c_3^{-1} d\right) \tag{28}$$

Proof:

Step 1. Define the Lyapunov candidate as follows

$$L_t(\varepsilon) = \frac{1}{2} c_3 \varepsilon^T \varepsilon \tag{29}$$

Taking gradient of $L_t(\varepsilon)$with respect to ε, we have

$$\nabla_\varepsilon L_t = c_3 \varepsilon = c_3\left(c_2 G_c^T x_p - \zeta\right) \tag{30}$$

For simplicity, we denote $\nabla_\varepsilon L_t$ as ∇L_t.

Step 2. Substituting (30) into u in (24), we achieve

$$u = -c_1 g_d c_3 \left(c_2 G_c^T x_p - \zeta\right) = -c_1 g_d \nabla L_t \tag{31}$$

Step 3. Substituting (31) into (22) to have the dynamic of $\dot{x}_p$ as follows

$$\dot{x}_p = \xi \nabla H_d - c_1 g_d G_c \nabla L_t - g_d G_c d \tag{32}$$

Step 4. Taking the time-derivative of ε in (26)

$$\dot{\varepsilon} = c_2 \dot{G}_c^T x_p + c_2 G_c^T \dot{x}_p - \dot{\zeta} \tag{33}$$

Step 5. Substituting (32), and $\dot{\zeta}$ in (25), into (33), we achieve the second dynamic:

$$\begin{aligned} \dot{\varepsilon} = \left(c_2 G_c^T \tilde{\xi} + c_1 g_d G_c^T\right) \nabla H_d - c_1 c_2 g_d G_c^T G_c \nabla L_t \\ - c_2 g_d G_c^T G_c d \end{aligned} \tag{34}$$

Step 6. From (33) and (34), the system can be summed up as follows:

$$\begin{aligned} &\begin{bmatrix} \dot{x}_p \\ \dot{\varepsilon} \end{bmatrix} \\ &= \begin{bmatrix} \xi & -c_1 g_d G_c \\ c_2 G_c^T \tilde{\xi} + c_1 g_d G_c^T & -c_1 c_2 g_d G_c^T G_c \end{bmatrix} \begin{bmatrix} \nabla H_d \\ \nabla L_t \end{bmatrix} \\ &- \begin{bmatrix} g_d G_c \\ c_2 g_d G_c^T G_c \end{bmatrix} d \end{aligned} \tag{35}$$

Step 7. The system (35) is still perturbed by the matched disturbance d. Taking the gradient of (28) with respect to ε, we have the following:

$$\nabla L_c = c_3 \varepsilon + \frac{1}{c_1} d = \nabla L_t + \frac{1}{c_1} d$$

As the result, we have ∇L_t has the form

$$\nabla L_t = \nabla L_c - \frac{1}{c_1} d \tag{36}$$

Step 8. Substituting (36) into (35), we achieve (27).

The proof is completed. ∎

Remark 4. From proposition 1, the input u in (13) is augmented with the additional state ζ, we recall (13) to conclude the final form of the input control law for the unperturbed system (12) as follows

$$\begin{cases} u_1 = u_{es} + u_{di} + u \\ u_{es} = G^+ \left[\nabla_q H - M_d M_t^{-1} \nabla_q H_d + J_2 \nabla_p H_d\right] \\ u_{di} = -K_V G^T \nabla_p H_d \\ u = -c_1 c_3 g_d \left(c_2 G_c^T x_p - \zeta\right) \end{cases} \tag{37}$$
$$\dot{\zeta} = G_c^T \left(c_2 \hat{\xi} - c_1 g_d I_n\right) \nabla H_d + c_2 \dot{G}_c^T x_p$$

Where the parameters of the control law (37) is defined in (13), and satisfies the condition in Proposition 2. The visualize structure of the proposed method can be shown in the Fig. 2.

In the next section, a stability analysis is presented, along with an assumption and a lemma, to support the proof of stability for the proposed method.

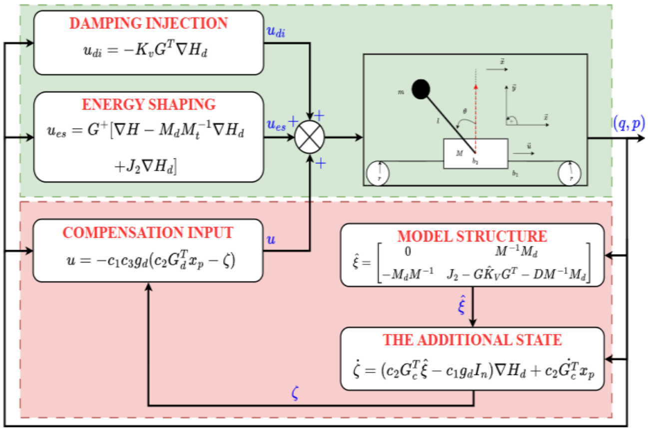

Fig. 2. The control structure of iIDA-PBC

B. Stability Analysis

Assumption 1: The matrix $\tilde{\xi}(q, p)$ satisfies the following

a) The modelling error $\tilde{\xi}$ is assumed to be associated to only the term R_d, this means that $\hat{\xi}(q, p)$ has the form

$$\hat{\xi}(q, p) = J_d(q, p) - \hat{R}_d(q) \tag{38}$$

In which, the form of $\hat{R}_d(q) = \begin{bmatrix} 0_{2\times2} & 0_{2\times2} \\ 0_{2\times2} & G\hat{K}_V G^T \end{bmatrix}$.

b) There exists a boundary constant $\lambda > 0$ such that

$$\|\tilde{\xi}(q, p)\| < \lambda \tag{39}$$

Recall that $\tilde{\xi}(q, p) = \xi(q, p) - \hat{\xi}(q, p)$.

Remark 5. The modeling error in equation (38) is a specific type that can be compensated for using the proposed method. If $K_V \neq \hat{K}_V$, then the input u will compensate for the error between the two parameters. For instance, a system with $K_V = 3$ and $\hat{K}_V = 25$ will exhibit the same response as a system with $K_V = 25$. Considering this, we make an additional assumption regarding the boundary of the system error to derive the conditions on the controller parameters $\{c_1, c_2, c_3\}$that ensure robustness against modeling errors.

Lemma 1: The term R_d defined in (16) has the rank 1, there exist a unitary matrix $U(q) = [U_2(q) \quad U_1(q)] \in \mathbb{R}^{4\times4}$ such that

$$R_d = \begin{bmatrix} 0 & 0 \\ 0 & GK_V G^T \end{bmatrix} = U(q) diag\{0,0,0,\lambda_1\} U^T(q) \tag{40}$$

We achieve the following claim

$$\tilde{\xi}(q, p) U_2(q) = 0_{4\times3} \tag{41}$$

Proof:

Calculating R_d

$$R_d(q) = \begin{bmatrix} 0 & 0 & 0 & 0 \\ 0 & 0 & 0 & 0 \\ 0 & 0 & K_V & \frac{K_V}{l} \cos\theta \\ 0 & 0 & \frac{K_V}{l} \cos\theta & \left(\frac{K_V}{l} \cos\theta\right)^2 \end{bmatrix} \tag{42}$$

The non-zero eigenvalues of $R_d(q)$ are

$$\lambda_1 = K_V\left(1+\frac{cos^2\theta}{l^2}\right) \tag{43}$$

And the decomposition of unitary of the square matrix in (42) is of the form

$$U_1(q) = \begin{bmatrix} 0 & 0 & \frac{1}{\sqrt{\frac{cos^2\theta}{l^2}+1}} & \frac{cos\,\theta}{l\sqrt{\frac{cos^2\theta}{l^2}+1}} \end{bmatrix}^T$$
$$U_2(q) = \begin{bmatrix} I_{2\times2} & 0_{2\times1} & 0_{2\times1} \\ 0_{1\times2} & -\frac{cos\,\theta}{l\sqrt{\frac{cos^2\theta}{l^2}+1}} & \frac{1}{\sqrt{\frac{cos^2\theta}{l^2}+1}} \end{bmatrix}^T \tag{44}$$

These resulted square matrix in (44) construct the unitary matrix verified by its property $U^TU = UU^T = I_{4\times4}$.

From (44), the claim from (40) and (41) is verified by computing.

The proof is completed. ■

Lemma 1 is used in the proof of the following proposition 2.

Proposition 2: The following properties are given by the system (27):

a) If $\tilde{\xi}(x_p)$ is bounded, for which $\lambda \neq 0$,the system is asymptotically stable at $(x_p^*, \zeta^*) = (x_p^*, c_2G_c^Tx_p^* - c_1^{-1}c_3^{-1}d)$ such that the gains c_1, c_2 of the controller satisfy as follows

$$\frac{c_1}{c_2} > \frac{\lambda^2}{4\lambda_1\lambda_d} \tag{45}$$

Where $\lambda_d = argmin\{g_d(\theta)\}$, $\lambda_1$in (43).

b) If $\tilde{\xi}(x_p)$ is zero, for which λ becomes zero, the system is asymptotically stable for $c_1, c_2 > 0$ at the equilibrium point $(x_p^*, \zeta^*) = (x_p^*, c_2G_c^Tx_p^* - c_1^{-1}c_3^{-1}d)$.

Proof:

Step 1. Taking the time-derivative of the Lyapunov function candidate $L(x_p,\varepsilon) = H_d(x_p) + L_c(\varepsilon)$.

$$\dot{L} = \nabla H_d\dot{x}_p + \nabla L_c\dot{\varepsilon} \tag{46}$$

Step 2. Substituting (27) into (46), we achieve

$$\dot{L} = -\begin{bmatrix}\nabla H_d \\ \nabla L_c\end{bmatrix}^T \begin{bmatrix} R_d & -\frac{1}{2}c_2\tilde{\xi}^TG_c \\ -\frac{1}{2}c_2G_c^T\tilde{\xi} & c_1c_2g_dG_c^TG_c \end{bmatrix} \begin{bmatrix}\nabla H_d \\ \nabla L_c\end{bmatrix} \tag{47}$$

Step 3. Invoke lemma 1, the term $R_d(q)$ can be expressed as

$$R_d = U_1(q)\lambda_1U_1^T(q) \tag{48}$$

We transform the modelling error $\tilde{\xi}$ in (46) as the form

$$\begin{gathered}\tilde{\xi} = \tilde{\xi}I = \tilde{\xi}[U_2 \quad U_1][U_2^T \quad U_1^T]^T \\ \Leftrightarrow \tilde{\xi} = \tilde{\xi}U_2U_2^T + \tilde{\xi}U_1U_1^T\end{gathered} \tag{49}$$

Recall from (41) that $\tilde{\xi}(q,p)U_2(q) = 0_{4\times3}$. We have:

$$\tilde{\xi} = \tilde{\xi}U_1U_1^T \tag{50}$$

Step 4. Substituting (48), (49), and (41) into (47), the expression of (47) is equivalent to the following

$$\dot{L} = -\begin{bmatrix}U_1^T\nabla H_d \\ \nabla L_c\end{bmatrix}^T \begin{bmatrix} \lambda_1 & -\frac{1}{2}c_2U_1^T\tilde{\xi}^TG_c \\ -\frac{1}{2}c_2G_c^T\tilde{\xi}U_1 & c_1c_2g_dG_c^TG_c \end{bmatrix} \times \begin{bmatrix}U_1^T\nabla H_d \\ \nabla L_c\end{bmatrix} \tag{51}$$

Step 5. We define the square matrix in (51) as follows

$$R_1(q) \triangleq \begin{bmatrix} \lambda_1 & -\frac{1}{2}c_2U_1^T\tilde{\xi}^TG_c \\ -\frac{1}{2}c_2G_c^T\tilde{\xi}U_1 & c_1c_2g_dG_c^TG_c \end{bmatrix} \tag{52}$$

$R_1(q)$ can be expressed as follows

$$R_1(q) = \begin{bmatrix} I_{1\times1} & 0_{1\times4} \\ 0_{2\times1} & G_c^T \end{bmatrix} \begin{bmatrix} \lambda_1 & -\frac{1}{2}c_2U_1^T\tilde{\xi}^T \\ -\frac{1}{2}c_2\tilde{\xi}U_1 & c_1c_2g_d \end{bmatrix} \times \begin{bmatrix} I_{1\times1} & 0_{1\times2} \\ 0_{4\times1} & G_c \end{bmatrix} \tag{53}$$

Step 6. Defining the new square matrix in (53)

$$R_t(q) \triangleq \begin{bmatrix} \lambda_1 & -\frac{1}{2}c_2U_1^T\tilde{\xi}^T \\ -\frac{1}{2}c_2\tilde{\xi}U_1 & c_1c_2g_d \end{bmatrix} \tag{54}$$

It shows that $\dot{L} \leq 0$ by ensuring that $R_t(q) > 0$. The conditions that ensure $R_t(q) > 0$ are as follows

$$\begin{cases}\lambda_1 > 0 \\ c_1c_2g_d\lambda_1 - \frac{1}{4}c_c^2\tilde{\xi}U_1U_1^T\tilde{\xi}^T > 0\end{cases} \tag{55}$$

Since $\lambda_1 = K_V\left(1+\frac{cos^2\theta}{l^2}\right)$, adjusting $K_V > 0$ holds the first condition in (55). For the second term, the condition holds for any c_1, c_2 satisfying the following

$$\frac{c_1}{c_2} > \frac{\lambda^2}{4\lambda_1\lambda_d} > \frac{\|\tilde{\xi}\|^2}{4\lambda_1\|g_d\|} \geq \ldots \geq \frac{\tilde{\xi}U_1U_1^T\tilde{\xi}^T}{4\lambda_1g_d} \tag{56}$$

Remark 6. When the system (27) satisfies the condition (56), we can conclude that $\dot{L} \leq 0$ where $R_1(q) \succ 0$. Applying Lasalle's theorem, the system converges to the largest invariant set defined by $U_1^T\nabla H_d = 0$ and $\nabla L_c = 0$. We have in (27) that $\dot{x}_p = \xi\nabla H_d$ if $\nabla L_c = 0$. Since $\dot{x}_p = \xi\nabla H_d$ is the closed-loop system of the form (3), so that $x_p^* = (q^*, 0)$ is an asymptotically stable equilibrium point. Furthermore, as $\nabla L_c = 0$ we have

$$\begin{aligned}\nabla L_c = 0 \Leftrightarrow c_3\varepsilon^* + \frac{1}{c_1}d = 0 \Leftrightarrow c_3(c_2G_c^Tx_p^* - \zeta^*) + \frac{1}{c_1}d \\ = 0 \Rightarrow \zeta^* = c_2G_c^Tx_p^* + c_1^{-1}c_3^{-1}d\end{aligned}$$

a) If $\xi(x_p) = \hat{\xi}(x_p) \Leftrightarrow \tilde{\xi}(x_p) = 0$, the constant $\lambda = 0$. In which, the condition (56) becomes true for any choice of $c_1 > 0$ and $c_2 > 0$. The conclusion about the equilibrium point is stated in the same way as in Remark 6.

The proof is completed. ■

C. Implementation Procedure for iIDA-PBC

We summarize the design procedure of the iIDA-PBC for the UIPS in 4 steps (Fig. 3):

Step 1. From the open-loop system (9), applying feedback equivalence transform (10), we obtain (11), which can be interpreted as a PCH system (12).

Step 2. Match the PCH system (12) with the desired system (13) to derive the control law (13) and the PDEs (14), (15), which must be solved to obtain the new energy function (17).

Step 3. Solve the PDEs (14) and (15) by following the steps in Table II to derive the parameters for the IDA-PBC control law (13), The resulting closed-loop system (16) admits the equilibrium point at $(q, p) = (q^*, 0)$ when $d = 0$.

Step 4. Using Proposition 1, we derive the iIDA-PBC control law (37) for the perturbed system (22) to become (27). With the choice of controller parameters from Proposition 2, the newly obtained closed-loop system (27) admits an equilibrium point at $\left(x_p^*, \zeta^*\right) = \left(x_p^*, c_2 G_c^T x_p^* + c_1^{-1} c_3^{-1} d\right)$ where $x_p^* = (q^*, 0)$.

Remark 7. The tuning procedure of the IDA-PBC parameters is summarized as follows, and it is primarily based on empirical observations and practical insights.

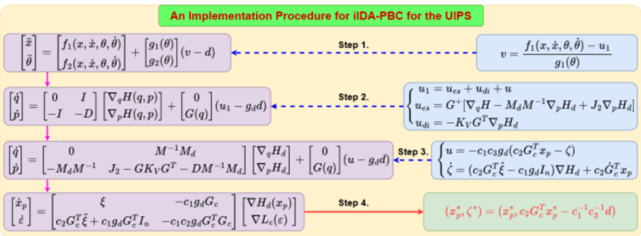

Fig. 3. The iIDA-PBC design procedure for the UIPS

Fig. 4 presents a block diagram outlining the process of tuning the parameters of the IDA-PBC controller for both simulation and experimental setups. The steps in the diagram are designed to be clear and straightforward, ensuring an intuitive understanding of the process.

The parameter evaluation is based on the system's response characteristics, including overshoot, settling time, and oscillations. Each parameter corresponds to a specific aspect of the system's dynamics. As described in equation (17), adjusting k increases the gain in the kinetic energy equation, specifically affecting the inertia matrix M_d. Modifying P impacts the gain in the cart's position term in the potential energy equation, while tuning K_V influences the dissipation properties of the system, as outlined in equation (37).

Once the steps are completed and the user is satisfied with the system's response based on the obtained parameters, the tuning process can be concluded.

Remark 8. The tunning of c_1, c_2, and c_3 for the dynamic state feedback u and the additional state ζ is straightforward, as described in the control law (37).

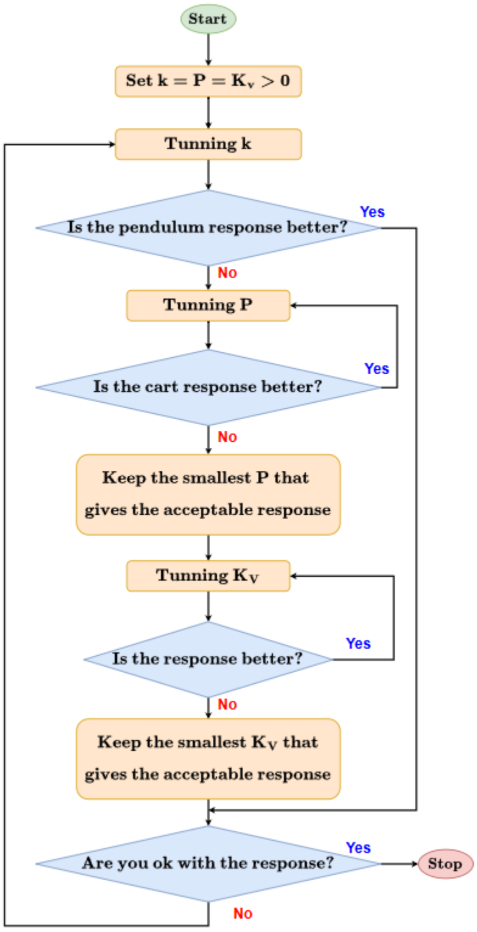

Fig. 4. The experiment tunning procedure for the IDA-PBC controller

$$\begin{cases} u = -c_1 c_3 g_d \left(c_2 G_c^T x_p - \zeta\right) \\ \dot{\zeta} = G_c^T \left(c_2 \dot{\xi} - c_1 g_d I_n\right) \nabla H_d + c_2 \dot{G}_c^T x_p \end{cases}$$

- Modify c_1 ↑↓ to regulate the amplitude and the convergence rate of ζ ↑↓ and u ↑↓.
- Adjust c_2 ↑↓ if the convergence rate and the amplitude of ζ ↑↓ are insufficient. Besides, the convergence rate of u ↑ ↓ is also affected by c_2.
- Tune c_3 ↑↓ to directly control the convergence rate of the input u ↑↓ and the steady-state value of ζ.

We have that $\zeta^* = c_2 G_c^T x_p^* - c_1^{-1} c_3^{-1} d$, so adjusting c_1, c_3 will affect the steady-state value of the additional state ζ. Moreover, both c_1 and c_3 influence the convergence rate of u, but c_3 is specifically dedicated to adjusting it, therefore, it is preferable to adjust the gain of u using c_3. The compensation input u will converge to $u^* = c_1 c_3 g_d(0) \zeta^*$.

Increasing c_2 results in a higher peak of ζ during the transient phase, while its steady-state value remains unchanged.

IV. RESULTS

A. Simulation Results

The simulations are performed in MATLAB with the initial states of the system set as $\left(x, \theta, \dot{x}, \dot{\theta}\right) = (0.1, 0.3, 0, 0)$ (Fig. 5).

The system's parameters are:

$g = 9.81, r = 0.019099, R = 0.32828, B = 5.4207 \times 10^{-4}$
$kt = 0.077166, l = 0.12419, b_1 = 0.85151, b_2 = 2.0887 \times 10^{-6}$
$J = 4.6843 \times 10^{-5}, m = 0.040796, M = 0.029392.$

1) Case study 1: Tuning Control Parameters for IDA-PBC

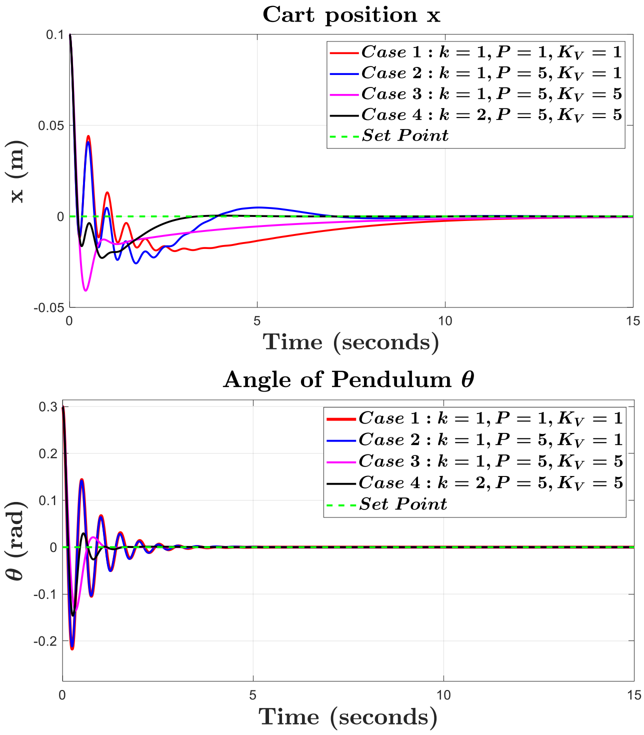

Fig. 5. The system's response under different parameter configurations.

The system's response with the IDA-PBC controller shows noticeable improvement as the parameters are adjusted following the guidelines in Remark 7. A comparison between case 1 and case 4 reveals that, although the overshoot in case 4 is comparable to that in case 1, case 4 demonstrates superior performance with significantly reduced oscillations and a shorter settling time.

By following the parameter tuning procedure outlined in remark 7, the input response of the system shown in Fig. 6 and its error metrics with respect to the set point from Table III, demonstrates that suboptimal parameter choices, as seen in case 1 and case 2, lead to increased oscillations and longer settling times compared to the improved tuning parameters in case 3 and case 4. Furthermore, Fig. 6 illustrates that the simulated input results produce voltage values suitable for practical implementation in real-world systems, assuming a reasonable initial state of the system. These findings validate the feasibility and applicability of the proposed control method in practice.

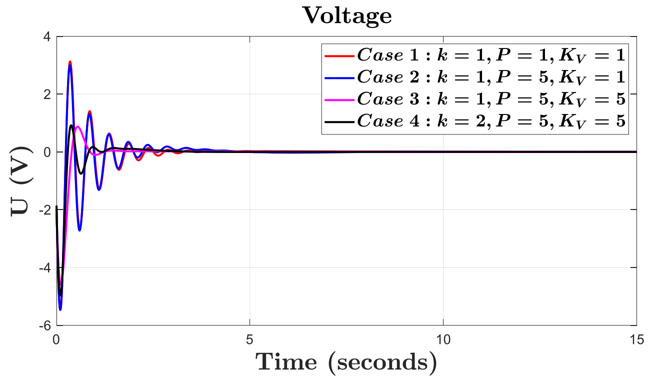

Fig. 6. The input value in each parameter configuration

2) Case study 2: Rejection of Matched Disturbances Using the iIDA-PBC Method when $\xi = \hat{\xi}$

The controller parameters are set as $k = 5, P = 10$ and, $K_V = \hat{K}_V = 25$ while the parameters $\{c_1, c_2, c_3\}$ are tuned, and the initial additional state ζ is zero. The disturbance gain constant $d = 0.1$ is applied at the 15th second during the 30-second simulation.

In Fig. 7, case 1, with the parameters $c_1 = c_2 = c_3 = 0$, corresponds to the system controlled only by the IDA-PBC. In this case, with the absence of $d = 0.1$, the pendulum stabilizes at $\theta^* = 0$, while the cart's position shifts according to equation (21):

$$x^* = \frac{2g_d(0)d}{Pk} = \frac{2\dfrac{1}{M + J/r}d}{Pk} = \frac{2\dfrac{0.1}{0.029392 + \dfrac{4.6843 \times 10^{-5}}{0.019099}}}{10 \times 5} = 0.1256$$

It can be observed that increasing P and k in the IDA-PBC method helps to reduce the cart's shifted position. However, this approach is not feasible, as the shifted position becomes zero only if P or k approaches infinity.

The remaining cases demonstrate that the proposed method can effectively reject the constant matched disturbance. The results show that (x^*, θ^*) converges to zero within approximately 3 seconds, when $d \neq 0$. Adjusting c_1, c_2 and c_3 according to Remark 8 reveals that increasing these parameters reduces the amplitude of oscillations under disturbance. Specifically, all parameters contribute to amplitude reduction when increased.

TABLE III. ERROR METRICS COMPARISON TABLE

	NMAE (%)				NRMSE (%)			
Case	1	2	3	4	1	2	3	4
x	0.069	0.040	0.042	0.024	0.108	0.090	0.081	0.079
θ	0.0175	0.0174	0.011	0.010	0.065	0.064	0.0619	0.0566

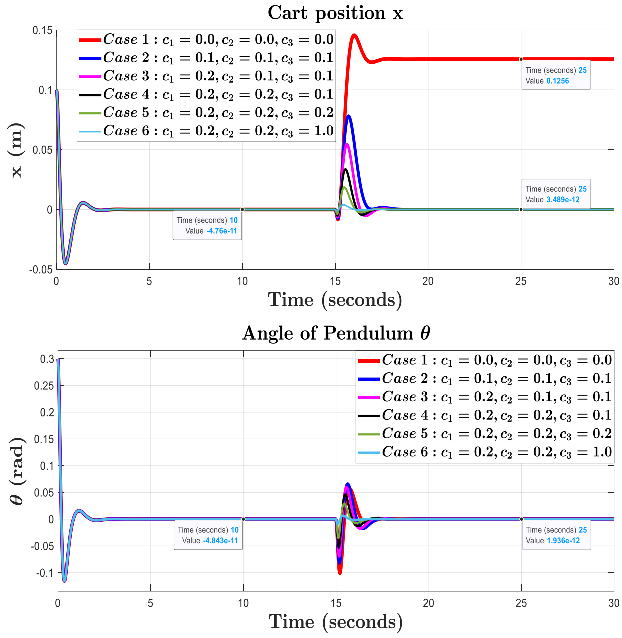

Fig. 7. The system's response under different parameter configurations

In Fig. 8, the behavior of the proposed additional state ζ is depicted. In case 1, $\zeta = 0$, as expected from equation (37), given its initial value is zero. At the beginning, when $d = 0$, it is observed that in case 2 and case 3, with c_2 unchanged, the oscillations have similar amplitudes and convergence rates. However, in case 4, 5 and 6, increasing c_2 results in larger oscillation amplitudes compared to the first two cases, though the convergence rates remain similar (as noted in Remark 8).

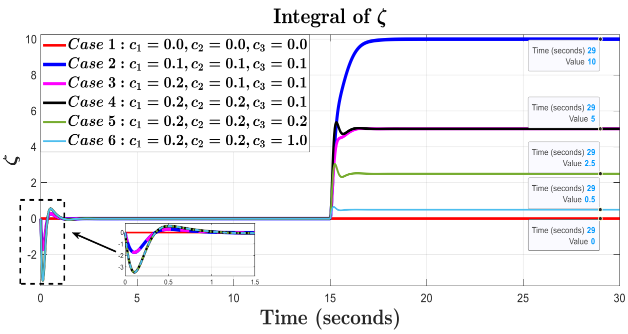

Fig. 8. The value of the integral state of the controller

When $d \neq 0$, changes in c_1 and c_3 (increased across case 2, 3, 5 and 6) lead to a reduction in the steady-state value of ζ, as highlighted in Remark 6. In case 3 and case 4, increasing c_2 reduces the settling time of case 4, as its larger c_2 value accelerates convergence. Both cases, however, converge to the same value of $\zeta = 5$. The steady-state values of $\zeta$are calculated as follows:

- Case 2: $\zeta^* = \frac{d}{c_1 c_3} = \frac{0.1}{0.1\times 0.1} = 10$
- Case 3: $\zeta^* = \frac{d}{c_1 c_3} = \frac{0.1}{0.2\times 0.1} = 5$
- Case 4: $\zeta^* = \frac{d}{c_1 c_3} = \frac{0.1}{0.2\times 0.2} = 2.5$
- Case 5: $\zeta^* = \frac{d}{c_1 c_3} = \frac{0.1}{0.2\times 1.0} = 0.5$

These values are confirmed to be accurate when compared with the simulation results in Fig. 8.

In Fig. 9, since $\zeta \to \zeta^*$ and $(x^*, \theta^*) \to 0$, the proposed control law ensures $u \to u^* = c_1 c_3 g_d(0)\zeta^*$ (as noted in Remark 8). Verification shows that case 2, 3, 4, 5 and 6 yield $u^* = 3.14$ for their respective parameter sets. For instance, in case 6, we have

$$u^* = c_1 c_3 g_d(0)\zeta^* = c_1 c_3 \frac{1}{M + J/r}\zeta^*$$
$$= 0.2\times 1.0\times \frac{1}{0.029392 + \dfrac{4.6843\times 10^{-5}}{0.019099}}\times 0.5 = 3.1402$$

Additionally, tuning $\{c_1, c_2, c_3\}$ impacts the convergence rate of u. From previous results in Fig. 7 and Fig. 8, it is recommended to adjust c_3 to improve the convergence rate of u without affecting the ζ's convergence rate. In contrast, c_1 and c_2 are better suited for adjusting the metrics of ζ.

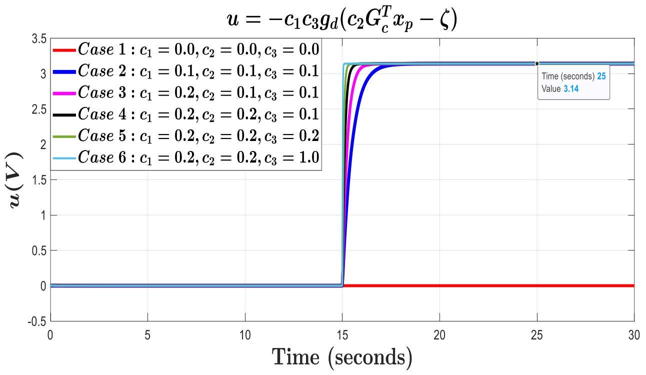

Fig. 9. Compensation input under varying parameters

Fig. 10 shows the total input value in the UIPS, for which $u_1 = u_{es} + u_{di} + u$. When there is no disturbance ($d = 0$), the responses in all cases converge to zero and are identical. When $d \neq 0$, in case 1, where $u = 0$, although changes in u_1 occur due to the reaction of u_{es} and u_{di}, the disturbance cannot be rejected because this case uses only the IDA-PBC controller (as shown in Fig. 7, and the formula $u_1 = u_{es} + u_{di}$). In the other cases, the proposed controller with different parameters (Fig. 10) shows that u_1 is capable of rejecting the constant matched disturbance and remains within a practical range suitable for real-world configuration. This result forms the basis for applying the method to the practical model.

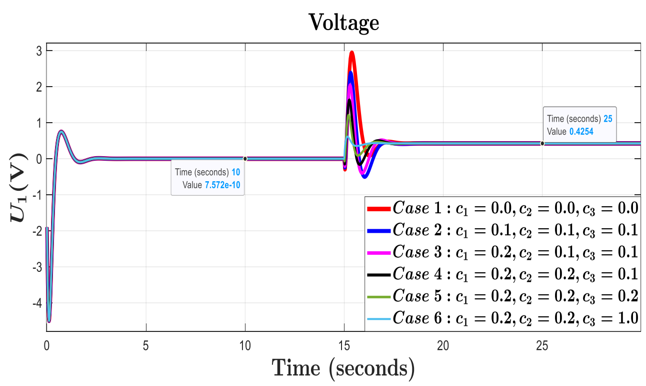

Fig. 10. The input value in each parameter configuration

3) Case study 3: Rejection of Matched Disturbances Using the iIDA-PBC Method when $\xi \neq \hat{\xi}$

The controller parameters are $\{c_2, c_3\} = \{0.2, 1\}$ and $\{k, P\} = \{5, 10\}$ while the parameters $\{c_1, K_V, \hat{K}_V\}$ are tunned, and the initial additional state ζ is zero.

In this Case Study 3, we examine the scenario where the K_V of the IDA-PBC controller differs from $\hat{K}_V$, which is used in the compensation input u of $\hat{\xi}$ from the control law (37). The cases considered are pairs of cases 1 and 2, followed by cases 3 and 4, and finally cases 5 and 6. Across these pairs, the parameter c_1 is gradually increased to ensure that the system response matches the desired system response ($\xi \rightarrow \hat{\xi}$).

For example, in case 1, $K_V = 3$, and $\hat{K}_V = 25$ is the desired value. We examine the parameter c_1 in Proposition 2, specifically in (56). However, we do not calculate λ, $\lambda_1$or λ_d, instead, we gradually increase c_1. The methods NMAE, and NRMSE are used to evaluate whether the achieved response matches the desired system. We aim to analyze the results across all paired cases as follows:

Case 1 aims to achieve a response similar to that of Case 2, while case 3 is expected to produce an output identical to case 4. Similarly, in the final pair, the system response in case 5 is expected to closely resemble that in case 6.

Analyzing c_1 across the case pairs 1-2, 3-4, and 5-6 in Fig. 11 and Fig. 12 demonstrates that increasing c_1 reduces the deviation between the actual system response and the desired response. The evaluation of system performance as c_1 is increased, following condition (56), is conducted using the NMAE, and NRMSE methods, as summarized in Table IV below.

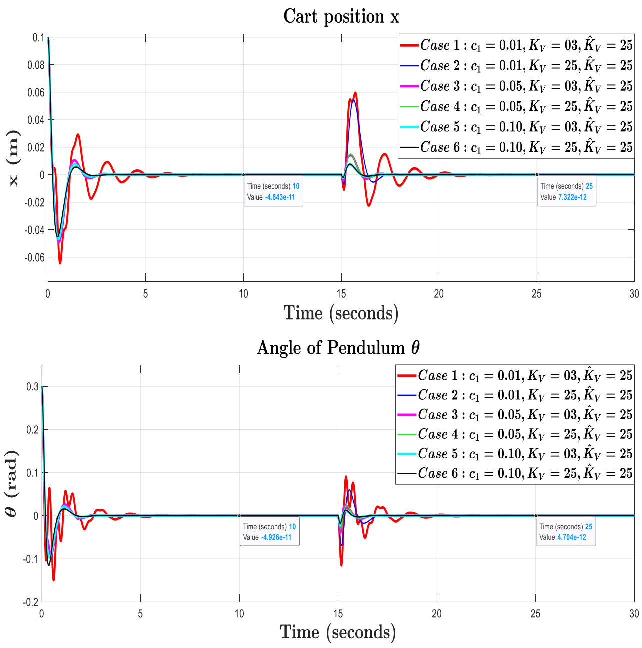

Fig. 11. The system's response under different parameter configurations

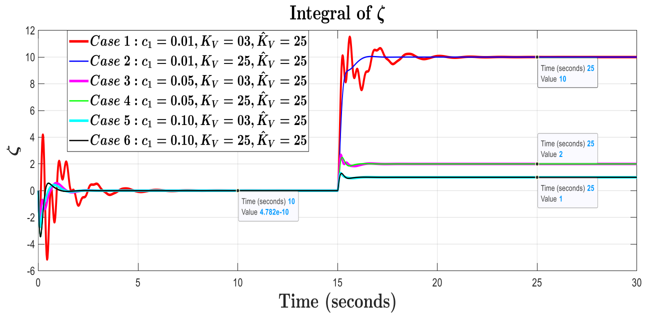

Fig. 12. The value of the integral state of the controller

TABLE IV. ERROR METRICS COMPARISON TABLE

Case	NMAE(%)			NRMSE(%)		
	1-2	3-4	5-6	1-2	3-4	5-6
x	0.0168	0.0025	0.0012	0.038	0.0089	0.0046
θ	0.0130	0.0027	0.0013	0.038	0.0117	0.0059
ζ	0.0148	0.0070	0.0041	0.043	0.0337	0.0222

(Note: Smaller error percentages in Table IV indicate higher accuracy.**)**

Increasing c_1 reduces the error between the output response of the system and the desired closed-loop response. Furthermore, although there is a mismatch in K_V, the system response in cases 1, 3, and 5 demonstrates that both x and θ converge to 0, while ζ successfully converges to the corresponding value, as explained in Remark 6 and in the previous case study.

From Fig. 13, the simulated input values of the system, both when $K_V = \hat{K}_V$ and $K_V \neq \hat{K}_V$, align well with real-world hardware conditions. For example, if the motor's power supply is 12V, the input values shown in the figure remain within a practical range of approximately -4V to +4V, demonstrating the controller's suitability for practical implementation in the practical UIPS system.

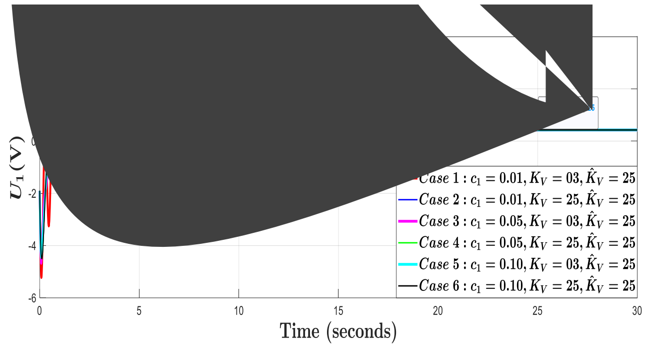

Fig. 13. The input value in each parameter configuration

4) Case study 4: Rejection of nonconstant Matched Disturbances using iIDA-PBC

The controller parameters are fixed for $\{c_1, c_2\} = \{1, 0.2\}$ and $\{k, P, K_V = \hat{K}_V\} = \{5, 10, 25\}$ while the parameters c_3 are tunned, and the initial additional state ζ is zero.

In this case study, the authors introduce an input disturbance $d = 0.2\,sin(2t)$ to evaluate the impact of a non-constant matched disturbance to the response of the closed-loop system (27).

To handle this disturbance, c_3 is adjusted to minimize the steady-state error of ζ while enhancing the convergence

It can be observed that case 1 and case 3 correspond to the IDA-PBC controller, while case 2 and case 4 represent the proposed iIDA-PBC controller to handle the constant matched disturbance d.

The disturbance is applied at the 15th second of a total 60-second dataset. The authors introduce an additional voltage v_d of 2 volts, corresponding to a disturbance calculated as follows:

$$d = \frac{k_t}{R} v_d = \frac{0.065}{0.7878} \times (-2) = -0.165$$

The calculated d is used to estimate the expected shifted equilibrium point of the system and compare it to the actual one in the practical UIPS.

In Fig. 17, it can be observed that the cart position in all cases oscillates around 0 during the first 15 seconds, similar to the pendulum angle. This indicates that the system remains stable around the equilibrium point at the origin. At the 15th second, when the disturbance d is applied by adding a voltage of $v_d = -2$ (volts), the following behavior is noted:

- **Case 1:** The cart position shifts by approximately 0.02 meters from the origin, and the pendulum's oscillation amplitude increases by around 0.02 radians compared to the first 15 seconds. However, both the cart and pendulum still oscillate around the equilibrium point. The displacement of the cart from the origin can be calculated as:

$$x^* = \frac{2g_d(0)d}{Pk} = \frac{2\frac{1}{M+J/r}d}{Pk} = \frac{2\frac{-0.165}{0.1293 + \frac{3.8704 \times 10^{-5}}{0.019099}}}{15 \times 5} = -0.0335$$

If we denote x_{shift} as the actual equilibrium shift point of the cart in Fig. 17, then $x_{shift} \approx x^*$.

- **Case 2:** From Fig. 17, it is evident that the cart and pendulum positions consistently maintain and oscillate around the equilibrium point at (0, 0). At the 15th second, when the disturbance is applied, the cart position deviates momentarily but returns to the original equilibrium point, continuing to oscillate around it while keeping the pendulum balanced. This demonstrates that the controller successfully rejects the constant matched disturbance d.

- **Case 3:** Similar conclusions can be drawn as in case 1, but with a different set of parameters for the IDA-PBC controller, as previously mentioned. The estimate of the displacement $x^*$is calculated as

$$x^* = \frac{2g_d(0)d}{Pk} = \frac{2\frac{1}{M+J/r}d}{Pk} = \frac{2\frac{-0.165}{0.1293 + \frac{3.8704 \times 10^{-5}}{0.019099}}}{10 \times 10} = -0.0251$$

As shown in Fig. 17, we clearly see that $x_{shift} \approx x^*$.

- **Case 4:** Similar to case 2, we conclude that the proposed method successfully rejects the constant matched disturbance d.

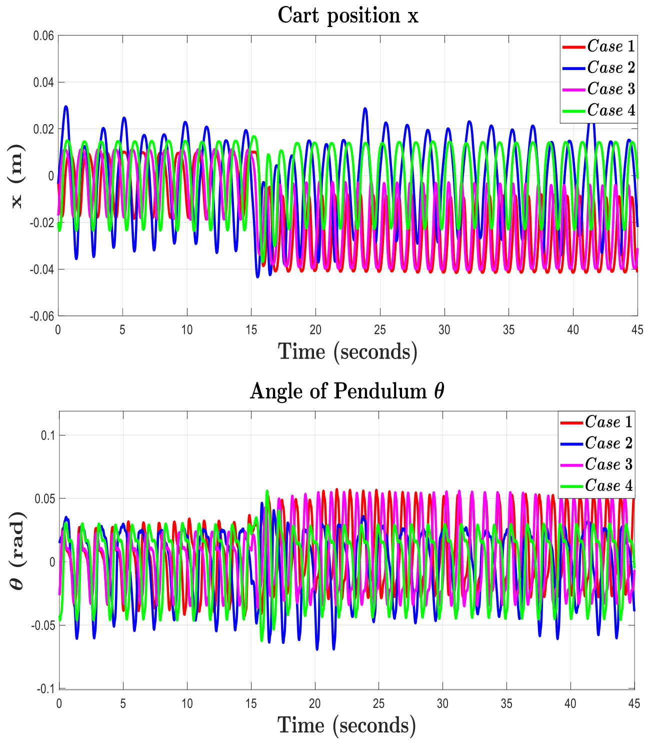

Fig. 17. The experimental system's response under different parameter configurations

The oscillations of the pendulum and cart around the equilibrium point suggest that the system is still influenced by unknown disturbances, certain electrical or mechanical dissipation components, or variations in the practical balance position of the upright pendulum. In practice, the equilibrium point may not align perfectly with the theoretical balance position but instead lies within a small neighborhood near it. This is because, in most practical UIPS setups, the initial position of the system is recorded by the rotary encoder at $\theta = \pm\pi$. Consequently, there is no guarantee that the actual balance point of the pendulum in practice corresponds precisely to $\theta = 0$. Therefore, improvements or new methods will be necessary in the future to address this issue.

The steady-state value of ζ in Case 2 and Case 4 can be approximated as:

$$\zeta^* = \frac{d}{c_1 c_3} = \frac{-0.165}{0.1 \times 0.2} = -8.25$$

The results in Fig. 18 demonstrate that this expected value closely matches the central value of ζ's oscillations in both cases after the disturbance d is introduced.

During the control process, the system input often operates within a narrow voltage range. Consequently, the supplied energy to the system (in this case a DC motor) is insufficient to generate the torque needed to move the pendulum cart, as this power from the voltage within the range in Fig. 19 is largely dissipated by friction in the electrical or mechanical components. The voltage range reveals that the system responds to input signals only when the voltage exceeds 2V, making this limitation the primary cause of the observed oscillations. When this voltage range is further narrowed through parameter adjustments, the amplitude of voltage variations increases significantly and occurs more rapidly, inducing strong oscillations in the belt connecting to the pendulum cart. This can result in premature wear or even complete failure of the practical system.

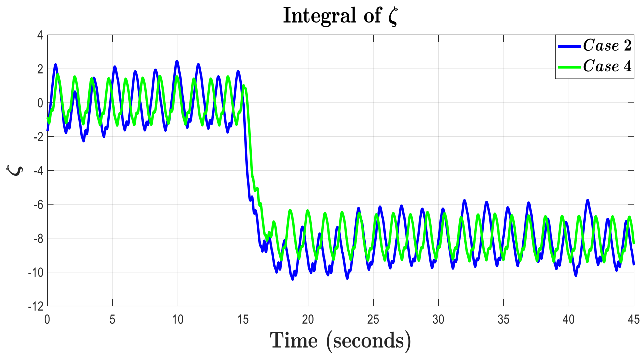

Fig. 18. The value of the integral state of the controller

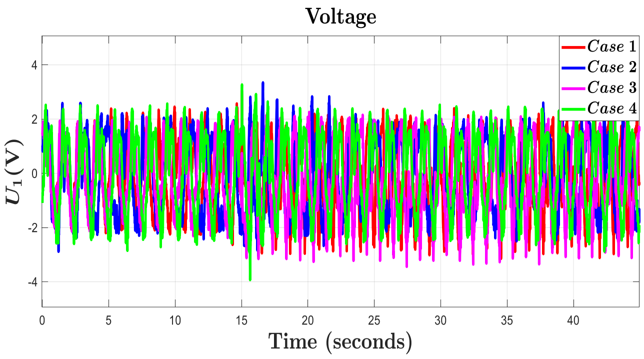

Fig. 19. The experimental input value of the system

The formula for predicting u based on ζ in case 2 and case 4, assuming the cart and pendulum velocities are zero, is given as:

$$u^* = c_1 c_3 g_d(0)\zeta^* = c_1 c_3 \frac{1}{M + J/r}\zeta^*$$
$$= 0.2 \times 1.0 \times \frac{1}{0.1293 + \dfrac{3.8704 \times 10^{-5}}{0.019099}} \times (-8.25) = 1.2564$$

In Fig. 20, it can be observed that the calculated voltage falls within the range affected by dissipative components, meaning the system is not influenced by this input. As a result, the oscillations arise due to the boundary regions where the input voltage exceeds the threshold required to affect the system response, leading to changes in its behavior.

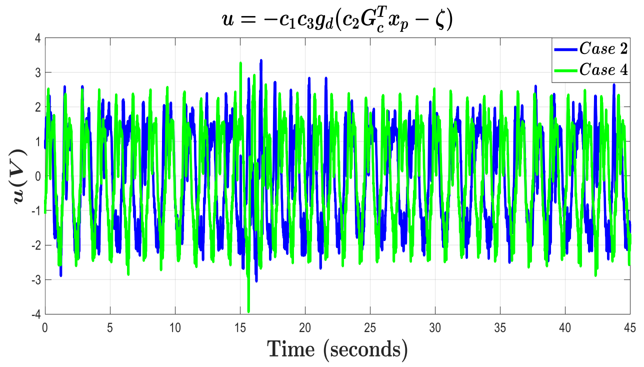

Fig. 20. The experimental compensation input

V. Conclusion

This study presents the design and application of both the traditional IDA-PBC and the proposed iIDA-PBC methods on the UIPS. By relaxing certain strict conditions in the previous researches in the controller design, the iIDA-PBC method can be extended to broader classes of systems that meet these requirements, as indicated in Remark 3. Compared to the conventional IDA-PBC, the iIDA-PBC more effectively rejects constant matched disturbances and avoids shifting the equilibrium point of the closed-loop system, as discussed in Section II.E and demonstrated in the simulation results (case study 2). Both simulation and experimental results confirm these advantages, highlighting the improved stability and effectiveness of the proposed approach.

However, the proposed method has limitations. It has only been validated for constant matched disturbances and does not perform as expected for other types, such as time-varying disturbances. For instance, as shown in case study 4, the iIDA-PBC fails to reject a time-varying matched disturbance generated using a sine wave signal. Additionally, the oscillations observed in experimental results are attributed to insufficient input supply, likely due to power loss under low-voltage conditions in the DC motor, static errors from state feedback, and potentially suboptimal choices of controller parameters.

Future research will focus on extending the iIDA-PBC method to handle unknown time-varying matched disturbances and unmatched disturbances, including unmodeled dynamics, parameter variations, and external factors such as friction, external forces, or environmental influences. Moreover, optimizing the tuning parameters of the IDA-PBC method to enhance performance and adaptability across various system conditions is a worthwhile direction for future studies. Additionally, maintaining the port-controlled Hamiltonian framework while expanding the operational range of the system, currently constrained by the limitations noted in Remark 3, remains a key objective. It is essential to avoid introducing unnecessary complexity or highly intricate partial differential equations, as solving these can be challenging. Striking a balance between simplicity and robustness will enhance the method's practicality, enabling its application in fields such as robotics, industrial automation, and transportation systems, where safety and efficiency are paramount.

Acknowledgment

We acknowledge the support of time and facilities from Ho Chi Minh City University of Technology, VNU-HCM for this study.

Conflicts of Interest

The authors declare that they have no conflict of interest.

References

[1] O. Saleem and J. Iqbal, "Phase-Based Adaptive Fractional LQR for Inverted-Pendulum-Type Robots: Formulation and Verification," *IEEE Access*, vol. 12, pp. 93185--93196, 2024, doi: 10.1109/ACCESS.2024.3415494.

[2] T. Li, X. Sun, Q. Wang, X. Guo, and Z. Han, "Control and stochastic dynamic behavior of Fractional Gaussian noise-excited time-delayed

inverted pendulum system," *Communications in Nonlinear Science and Numerical Simulation*, vol. 139, p. 108302, 2024, doi: 10.1016/j.cnsns.2024.108302.

[3] B. Tian, H. Peng, and T. Kang, "RBF-ARX model-based predictive control approach to an inverted pendulum with self-triggered mechanism," *Chaos, Solitons & Fractals*, vol. 186, p. 115291, 2024, doi: 10.1016/j.chaos.2024.115291.

[4] M. J. Mahmoodabadi, F. S. Hormozi, and M. Y. Ibrahim, "Optimal robust adaptive fuzzy controllers based on sliding surfaces for inverted pendulum systems," *Int. J. Dynam. Control*, vol. 12, pp. 4188-4204, 2024, doi: 10.1007/s40435-024-01486-5.

[5] T. V. A. Nguyen and N. H. Tran, "A T-S Fuzzy Approach with Extended LMI Conditions for Inverted Pendulum on a Cart," *Eng. Technol. Appl. Sci. Res.*, vol. 14, no. 1, p. 12670–12675, Feb. 2024, doi: 10.48084/etasr.6577.

[6] A. -V. Nguyen, V. -T. Ngo, W. -J. Wang, V. -P. Vu, T. -Q. Ngo, and A. Nguyen, "Fuzzy Logic Based LQG Controller Design for Inverted Pendulum On Cart," in *2021 International Conference on System Science and Engineering (ICSSE)*, 2021, doi: 10.1109/ICSSE52999.2021.9538411.

[7] T. Zhang, H. Zhang, and X. Xie, "Region Stability/Stabilization and H∞ Control for Discrete-Time Impulsive Takagi–Sugeno Fuzzy Systems," *IEEE Transactions on Fuzzy Systems*, vol. 32, no. 6, pp. 3410-3419, June 2024, doi: 10.1109/TFUZZ.2024.3372936.

[8] C. O'Kane and H. Han, "A Controller Based on a Class of Affine T–S Fuzzy Models Using Piece-Wise Lyapunov Functions," *International Journal of Fuzzy Systems*, vol. 26, pp. 1030-1045, 2024, doi: 10.1007/s40815-023-01651-6.

[9] H. Shen, Z. Zhang, F. Li, J. Wang, and J. Cao, "Passivity-Based Control of Fuzzy Singularly Perturbed Jump Systems Based on Semi-Markov Kernel Approach," *IEEE Transactions on Systems, Man, and Cybernetics: Systems*, pp. 1-11, 2024, doi: 10.1109/TSMC.2024.3450835.

[10] L. Zhang, Z. Li, Y. Li, and J. Dong, "State and Fault Interval Estimation for Discrete-time Takagi-Sugeno Fuzzy Systems via Intermediate Observer Base on Zonotopic Analysis," *IEEE Transactions on Fuzzy Systems*, pp. 1-6, 2024, doi: 10.1109/TFUZZ.2024.3459642.

[11] N. Han, H. Zhang, P. Lu, and Z. Liu, "Resonance response and chaotic analysis for an irrational pendulum system," *Chaos, Solitons & Fractals*, vol. 182, p. 114812, 2024, doi: 10.1016/j.chaos.2024.114812.

[12] Z. Liu, J. Gao, S. Ding, and X. Rao, "Chaotic behaviors and multiple attractors in a double pendulum with an external harmonic excitation," *Nonlinear Dynamics*, vol. 112, p. 1779–1796, 2024, doi: 10.1007/s11071-023-09140-z.

[13] J. He, L. Cui, J. Sun, P. Huang, and Y. Huang, "Chaotic dynamics analysis of double inverted pendulum with large swing angle based on Hamiltonian function," *Nonlinear Dynamics*, vol. 108, p. 4373–4384, 2022, doi: 10.1007/s11071-022-07455-x.

[14] X. Xia, J. Xia, M. Gang, Q. Zhang, and J. Wang, "Discrete Dynamics-Based Parameter Analysis and Optimization of Fuzzy Controller for Inverted Pendulum Systems Based on Chaos Algorithm," *Discrete Dynamics in Nature and Society*, vol. 1, p. 3639508, 2020, doi: 10.1155/2020/3639508.

[15] A. Wadi, S. Mukhopadhyay, and L. Romdhane, "Identifying Friction in a Nonlinear Chaotic System Using a Universal Adaptive Stabilizer," *IEEE Access*, vol. 10, pp. 39177-39192, 2022, doi: 10.1109/ACCESS.2022.3165081.

[16] S. Kwak and B.-J. Choi, "Design of Fuzzy Logic Control System for Segway Type Mobile Robots," *Int. J. Fuzzy Log. Intell. Syst.*, vol. 15, no. 2, pp. 126-131, 2022, doi: 10.5391/IJFIS.2015.15.2.126.

[17] T. -P. A. Perdicoúlis and P. L. Dos Santos, "The Secrets of Segway Revealed to Students: Revisiting the Inverted Pendulum," in *2018 13th APCA International Conference on Automatic Control and Soft Computing (CONTROLO)*, 2018.

[18] Y. Bao and H. Yang, "A three-dimensional spring-loaded inverted pendulum walking model considering human movement speed and frequency," *Bioinspir. Biomim*, vol. 19, no. 4, p. 046012, 2024, doi: 10.1088/1748-3190/ad48ee.

[19] B. Czaplewski, M. Bocian, and J. H. G. Macdonald, "Calibration of inverted pendulum pedestrian model for laterally oscillating bridges based on stepping behaviour," *Journal of Sound and Vibration*, vol. 572, p. 118141, 2024, doi: 10.1016/j.jsv.2023.118141.

[20] Y. -M. Chen, J. Hu, and M. Posa, "Beyond Inverted Pendulums: Task-Optimal Simple Models of Legged Locomotion," *IEEE Transactions on Robotics*, vol. 40, pp. 2582-2601, 2024, doi: 10.1109/TRO.2024.3386390.

[21] Z. Zhang, Q. Xiang, Y. Liu, H. Deng, J. Wang, and S. Guo, "Enhanced Rocker-based Inverted Pendulum Model for Human Dynamic Analysis in Lower Limb Exoskeletons," in *2024 IEEE International Conference on Mechatronics and Automation (ICMA)*, 2024, doi: 10.1109/ICMA61710.2024.10632970.

[22] B. T. van Oeveren, C. J. de Ruiter, P. J. Beek, and J. H. van Dieën, "The biomechanics of running and running styles: a synthesis," *Sports Biomechanics*, vol. 23, no. 4, p. 516–554, 2024, doi: 10.1080/14763141.2021.1873411.

[23] M. Safeea and P. Neto, "A Q-learning approach to the continuous control problem of robot inverted pendulum balancing," *Intelligent Systems with Applications*, vol. 21, p. 200313, 2024. doi: 10.1016/j.iswa.2023.200313.

[24] D. Zaborniak, K. Patan, and M. Witczak, "Design, Implementation, and Control of a Wheel-Based Inverted Pendulum," *Electronics*, vol. 13, no. 3, p. 514, 2024, doi: 10.3390/electronics13030514.

[25] D. Caradonna, M. Pierallini, C. D. Santina, F. Angelini, and A. Bicchi, "Model and Control of R-Soft Inverted Pendulum," *IEEE Robotics and Automation Letters*, vol. 9, no. 6, pp. 5102-5109, June 2024, doi: 10.1109/LRA.2024.3389348.

[26] P. Borja, "Interconnection and Damping Assignment Passivity-Based Control Without Partial Differential Equations," in *2024 UKACC 14th International Conference on Control (CONTROL)*, 2024, doi: 10.1109/CONTROL60310.2024.10532055.

[27] M. Mattioni, S. Monaco, and D. Normand-Cyrot, "IDA-PBC for LTI Dynamics Under Input Delays: A Reduction Approach," *IEEE Control Systems Letters*, vol. 5, no. 4, pp. 1465-1470, Oct. 2021, doi: 10.1109/LCSYS.2020.3040076.

[28] M. Mattioni, A. Moreschini, S. Monaco, and D. Normand-Cyrot, "Quaternion-Based Attitude Stabilization via Discrete-Time IDA-PBC," *IEEE Control Systems Letters*, vol. 6, pp. 2665-2670, 2022, doi: 10.1109/LCSYS.2022.3173509.

[29] R. P. Desai and N. S. Manjarekar, "Interconnection and damping assignment passivity-based control for dynamic steering position stabilization of an underactuated AUV," *Advanced Control for Applications: Engineering and Industrial Systems*, vol. 6, no. 3, p. e225, 2024, doi: 10.1002/adc2.225.

[30] A. K. Khalaji and M. Haghjoo, "Adaptive passivity-based control of an autonomous underwater vehicle," *Proceedings of the Institution of Mechanical Engineers, Part C: Journal of Mechanical Engineering Science*, vol. 236, no. 20, pp. 10563-10572, 2022, doi:10.1177/09544062221103818.

[31] Y. Wang, W. Yan, and J. Li, "Passivity-based formation control of autonomous underwater vehicles," *IET Control Theory & Applications*, vol. 6, no. 4, pp. 518-525, 2012, doi: 10.1049/iet-cta.2011.0354.

[32] Z. Liu, D. Theilliol, L. Yang, Y. He, and J. Han , "Interconnection and Damping Assignment Passivity-Based Control Design Under Loss of Actuator Effectiveness," *Journal of Intelligent & Robotic Systems*, vol. 100, p. 29–45, 2020, doi: 10.1007/s10846-020-01170-8.

[33] C. Souza, G. V. Raffo, and E. B. Castelan, "Passivity Based Control of a Quadrotor UAV," *IFAC Proceedings Volumes*, vol. 47, no. 3, pp. 3196-3201, 2014, doi: 10.3182/20140824-6-ZA-1003.02335.

[34] J. Jeong and M. J. Kim, "Passivity-based Decentralized Control for Collaborative Grasping of Under-Actuated Aerial Manipulators," in *2023 IEEE International Conference on Robotics and Automation (ICRA)*, 2023, doi: 10.1109/ICRA48891.2023.10160334.

[35] X. Zou, Z. Liu, B. Wang, W. Zhao, and Q. Dang, "Model-Free Control-Based Trajectory Tracking Control of a Tail-Sitter UAV in Hovering Mode," *IEEE Transactions on Instrumentation and Measurement*, vol. 73, pp. 1-20, 2024, doi: 10.1109/TIM.2024.3373081.

[36] M. -E. Guerrero-Sánchez, O. Hernández-González, G. Valencia-Palomo, F. -R. López-Estrada, A. -E. Rodríguez-Mata, and J. Garrido, "Filtered Observer-Based IDA-PBC Control for Trajectory Tracking of a Quadrotor," *IEEE Access*, vol. 9, pp. 114821-114835, 2021, doi: 10.1109/ACCESS.2021.3104798.

[37] J. C. Travieso-Torres *et al*., "Robust Combined Adaptive Passivity-Based Control for Induction Motors," *Machines*, vol. 12, no. 4, p. 272, 2024, doi: 10.3390/machines12040272.

[38] B. Fan, G. Huang, L. Sun, Y. Zhao, H. Zhou, and J. Wang, "Disturbance Rejection Control Method Based on Variable Damping and Port Controlled Hamiltonian with Dissipation Model for Induction Drive Motor," *International Journal of Precision Engineering and Manufacturing*, vol. 24, pp. 2009–2019, 2023, doi: 10.1007/s12541-023-00863-y.

[39] K. Baazouzi, S. Drid, and L. Chrifi-Alaoui, "Improving the Scalar Control of Induction Motor Using Passivity Based Control," in *2024 2nd International Conference on Electrical Engineering and Automatic Control (ICEEAC)*, 2024, doi: 10.1109/ICEEAC61226.2024.10576458.

[40] M. B. Astik, "Hardware implementation of interconnection and damping assignment passivity-based control for BLDC motor using microcontroller," *COMPEL-The international journal for computation and mathematics in electrical and electronic engineering*, vol. 42, no. 2, pp. 323-352, 2023, doi: 10.1108/COMPEL-10-2021-0367.

[41] D. S. Martinez-Padron *et al.*, "Trajectory Tracking via Interconnection and Damping Assignment Passivity-Based Control for a Permanent Magnet Synchronous Motor," *Appl. Sci.*, vol. 14, no. 17, p. 7977, 2024, doi: 10.3390/app14177977.

[42] Y. Belkhier *et al.*, "Experimental analysis of passivity-based control theory for permanent magnet synchronous motor drive fed by grid power," *IET Control Theory & Applications*, vol. 18, no. 4, pp. 495-510, 2023, doi: 10.1049/cth2.12574.

[43] E. W. Zurita-Bustamante, J. G. Rueda-Escobedo, and J. Schiffer, "Passivity-Based Conditions for Asymptotic Stability of Speed Control for Three-Phase and Dual Three-Phase Permanent Magnet Synchronous Motors," in *2023 62nd IEEE Conference on Decision and Control (CDC)*, 2023, doi: 10.1109/CDC49753.2023.10383817.

[44] M. Ryalat, D. S. Laila, and H. ElMoaqet , "Adaptive Interconnection and Damping Assignment Passivity Based Control for Underactuated Mechanical Systems," *International Journal of Control, Automation and Systems*, vol. 19, p. 864–877, 2021, doi: 10.1007/s12555-019-1019-z.

[45] M. Reza, J. Harandi, and H. D. Taghirad, "Adaptive interconnection and damping assignment passivity-based control for an underactuated cable-driven robot," *International Journal of Adaptive Control and Signal Processing*, vol. 35, no. 12, pp. 2487-2498, 2021, doi: 10.1002/acs.3332.

[46] W. Sirichotiyakul and A. C. Saticib, "Data-driven passivity-based control of underactuated mechanical systems via interconnection and damping assignment," *International Journal of Control*, vol. 96, no. 6, pp. 1448-1456, 2022, doi: 10.1080/00207179.2022.2051750.

[47] X. Liu *et al.*, "An Adaptive Controller Based on Interconnection and Damping Assignment Passivity-Based Control for Underactuated Mechanical Systems: Application to the Ball and Beam System," *Actuators*, vol. 12, no. 11, p. 408, 2023, doi: 10.3390/act12110408.

[48] P. Sistla *et al*., "Design and performance comparison of interconnection and damping assignment passivity-based control for vibration suppression in active suspension systems," *Journal of Vibration and Control*, vol. 27, no. 7-8, pp. 893-911, 2020, doi: 10.1177/1077546320933749.

[49] S. Zhang *et al*., "Passivity-based coupling control for underactuated three-dimensional overhead cranes," *ISA Transactions*, vol. 126, pp. 352-360, 2022.

[50] T. Zhang and J. Xia, "Interconnection and Damping Assignment Passivity-Based Impedance Control of a Compliant Assistive Robot for Physical Human–Robot Interactions," *IEEE Robotics and Automation Letters*, vol. 4, no. 2, pp. 538-545, 2019, doi: 10.1109/LRA.2019.2891434.

[51] Q. Zhang, Z. Xie, S. Kui, H. Yang, J. Minghe, and H. Cai, "Interconnection and damping assignment passivity-based control for flexible joint robot," in *Proceeding of the 11th World Congress on Intelligent Control and Automation*, 2014, doi: 10.1109/WCICA.2014.7053426.

[52] Q. Zhang and G. Liu, "Precise Control of Elastic Joint Robot Using an Interconnection and Damping Assignment Passivity-Based Approach," *IEEE/ASME Transactions on Mechatronics*, vol. 21, no. 6, pp. 2728-2736, Dec. 2016, doi: 10.1109/TMECH.2016.2578287.

[53] M. R. J. Harandi, S. A. Khalilpour, and H. Taghirad, "Robust IDA-PBC for a Spatial Underactuated Cable Driven Robot with Bounded Inputs," in *2021 29th Iranian Conference on Electrical Engineering (ICEE)*, 2021, doi: 10.1109/ICEE52715.2021.9544237.

[54] M. Khalid, "Passivity-Based Nonlinear Control Approach for Efficient Energy Management in Fuel Cell Hybrid Electric Vehicles," *IEEE Access*, vol. 12, pp. 84169-84188, 2024, doi: 10.1109/ACCESS.2024.3412888.

[55] S. Bedda, O. Kraa, M. Mohammedi, D. E. Zabia, I. Tegani, and M. K. Benbraika, "Optimization of Passivity-Based Controller for a Hybrid Vehicle Power Source using the Gray Wolf Algorithm," in *2024 8th International Conference on Image and Signal Processing and their Applications (ISPA)*, 2024, doi: 10.1109/ISPA59904.2024.10536755.

[56] F. M. Serra and C. H. D. Angelo, "Direct Power Control of a Shunt Active Power Filter Using a Modified IDA–PBC Approach With Integral Action," *IEEE Transactions on Circuits and Systems II: Express Briefs*, vol. 70, no. 6, pp. 1991 - 1995, June 2023.

[57] C. Zakaria, B. Smain, and T. Abdelhalim, "Two-Stage Converter Based on Droop Control and IDA-PBC in Islanded Mode," *2023 International Conference on Advances in Electronics, Control and Communication Systems (ICAECCS)*, pp. 1-5, 2023, doi: 10.1109/ICAECCS56710.2023.10105008.

[58] W. Gil-Gonzalez, O. Montoya, A. Herrera-Orozco, and F. Serra, "Adaptive IDA-PBC Applied to On-Board Boost Converter Supplying a Constant Power Load," in *2020 IEEE ANDESCON*, 2020, doi: 10.1109/ANDESCON50619.2020.9272078.

[59] M. Lapique, S. Pang, J. -P. Martin, S. Pierfederici, M. Weber, and S. Zaim, "Enhanced IDA-PBC Applied to a Three-Phase PWM Rectifier for Stable Interfacing Between AC and DC Microgrids Embedded in More Electrical Aircraft," *IEEE Transactions on Industrial Electronics*, vol. 70, no. 1, pp. 995-1004, Jan. 2023, doi: 10.1109/TIE.2022.3150079.

[60] M. Huang, F. Chen, Z. Zhang, W. Wu, Z. Yao, and L. Zhu, "Design of IDA-PBC Controller for LCL-Filtered Grid-Connected Inverter," in *IECON 2021 – 47th Annual Conference of the IEEE Industrial Electronics Society*, 2021, doi: 10.1109/IECON48115.2021.9589522.

[61] S. Pang, B. Nahid-Mobarakeh, S. Pierfederici, Y. Huangfu, G. Luo, and F. Gao, "Toward Stabilization of Constant Power Loads Using IDA-PBC for Cascaded LC Filter DC/DC Converters," *IEEE Journal of Emerging and Selected Topics in Power Electronics*, vol. 9, no. 2, pp. 1302-1314, April 2021, doi: 10.1109/JESTPE.2019.2945331.

[62] N. Khefifi, A. Houari, M. Machmoum, A. Saim, and M. Ghanes, "Generalized IDA-PBC Control Using Enhanced Decoupled Power Sharing for Parallel Distributed Generators in Standalone Microgrids," *IEEE Journal of Emerging and Selected Topics in Power Electronics*, vol. 9, no. 4, pp. 5069-5082, Aug. 2021, doi: 10.1109/JESTPE.2020.3034464.

[63] C. A. Beltrán, L. H. Diaz-Saldiernat, P. R. Martínez-Rodríguez, R. Cisneros, G. Vázquez-Guzmán, and D. Langarica-Córdoba, "Adaptive IDA-PBC for Output Voltage Regulation of a Fuel Cell Hybrid Storage System," in *2022 IEEE International Autumn Meeting on Power, Electronics and Computing (ROPEC)*, 2022, doi: 10.1109/ROPEC55836.2022.10018669.

[64] E. Franco, P. Arpenti, A. Donaire, and F. Ruggiero, "Integral IDA-PBC for Underactuated Mechanical Systems Subject to Matched and Unmatched Disturbances," *IEEE Control Systems Letters*, vol. 8, pp. 568-573, 2024, doi: 10.1109/LCSYS.2024.3399474.

[65] M. Yang, Y. Wang, X. Xiao, and Y. Li, "A Robust Damping Control for Virtual Synchronous Generators Based on Energy Reshaping," *IEEE Transactions on Energy Conversion*, vol. 38, no. 3, pp. 2146-2159, Sept. 2023, doi: 10.1109/TEC.2023.3260244.

[66] E. Franco and P. Borja, "Integral IDA-PBC of Underactuated Mechanical Systems with Actuator Dynamics and Uncertain Coupling," *IFAC-PapersOnLine*, vol. 58, no. 6, pp. 19-24, 2024, doi: 10.1016/j.ifacol.2024.08.250.

[67] M. Ryalat, D. S. Laila, and M. M. Torbati, "Integral IDA-PBC and PID-like control for port-controlled Hamiltonian systems," in *2015 American Control Conference (ACC)*, 2015, doi: 10.1109/ACC.2015.7172178.

[68] J. Ferguson, A. Donaire, and R. H. Middleton, "Integral Control of Port-Hamiltonian Systems: Nonpassive Outputs Without Coordinate Transformation," *IEEE Transactions on Automatic Control*, vol. 62, no. 11, pp. 5947-5953, Nov. 2017, doi: 10.1109/TAC.2017.2700995.

[69] J. Ferguson, A. Donaire, R. Ortega, and R. H. Middleton, "Matched Disturbance Rejection for a Class of Nonlinear Systems," *IEEE Transactions on Automatic Control*, vol. 65, no. 4, pp. 1710-1715, April 2020, doi: 10.1109/TAC.2019.2933398.

[70] J. Ferguson, R. H. Middleton, and A. Donaire, "Disturbance rejection via control by interconnection of port-Hamiltonian systems," in *2015 54th IEEE Conference on Decision and Control (CDC)*, 2015, doi: 10.1109/CDC.2015.7402279.

[71] A. Donaire *et al*., "Shaping the energy of mechanical systems without solving partial differential equations," in *2015 American Control Conference (ACC)*, 2015, doi: 10.1109/ACC.2015.7170921.

[72] R. Ortega *et al*., "Interconnection and damping assignment passivity-based control of port-controlled Hamiltonian systems," *Automatica,* vol. 38, no. 4, pp. 585-596, April 2002, doi: 10.1016/S0005-1098(01)00278-3.

[73] J. A. Acosta, R. Ortega, A. Astolfi, and A. D. Mahindrakar, "Interconnection and damping assignment passivity-based control of mechanical systems with underactuation degree one," *IEEE Transactions on Automatic Control,* vol. 50, no. 12, pp. 1936-1955, Dec. 2005, doi: 10.1109/TAC.2005.860292.

[74] J. G. Romero, A. Donaire, and R. Ortega, "Global Stabilisation of Underactuated Mechanical Systems via PID Passivity-Based Control," *arXiv e-prints arXiv: 1610.06999*, 2016.

[75] D. Cheng, A. Astolfi, and R. Ortega, "On feedback equivalence to port controlled Hamiltonian systems," *Systems & Control Letters,* vol. 54, no. 9, pp. 911-917, 2005, doi: 10.1016/j.sysconle.2005.02.005.

[76] M. Ryalat. *Design and implementation of nonlinear and robust control for Hamiltonian systems: the passivity-based control approach*. University of Southampton, Faculty of Engineering and the Environment, Doctoral Thesis, 2015.

[77] J. Ferguson, L. Zhou, S. Ahmed, and J. Scherpen, "On the Control-by-Interconnection interpretation of integral control for port-Hamiltonian systems," *IFAC-PapersOnLine,* vol. 58, no. 6, pp. 1-6, 2024, doi: 10.1016/j.ifacol.2024.08.247.

[78] P. Borja, J. Ferguson, and A. Schaft, "Interconnection Schemes in Modeling and Control," *IEEE Control Systems Letters,* pp. 2287-2292, 2023, DOI: 10.1109/LCSYS.2023.3286124.

[79] J. Ferguson, N. Sakata, and K. Fujimoto, "Input-to-State Stable Hybrid Momentum Observer for Mechanical Systems," *IEEE Control Systems Letters,* vol. 8, pp. 1361-1366, 2024, doi: 10.1109/LCSYS.2024.3410633.

[80] J. Ferguson and R. Mahony, "Passive interconnection interpretation of PID control," *IFAC-PapersOnLine,* vol. 56, no. 1, pp. 193-198, 2023, doi: 10.1016/j.ifacol.2023.02.033.

[81] K. Fujimoto, N. Sakata, I. Maruta, and J. Ferguson, "A Passivity Based Sliding Mode Controller for Simple Port-Hamiltonian Systems," *IEEE Control Systems Letters,* vol. 5, no. 3, pp. 839-844, 2021.

[82] E. Franco and M. Ryalat, "IDA-PBC with Dynamic Extension for Momenta Observation of Underactuated Mechanical Systems," in *2024 IEEE Conference on Control Technology and Applications (CCTA)*, 2024, doi: 10.1109/CCTA60707.2024.10666616.